Dynamic Treg interactions with intratumoral APCs promote local CTL dysfunction

Christian A. Bauer, Edward Y. Kim, Francesco Marangoni, Esteban Carrizosa, Natalie M. Claudio, and Thorsten R. Mempel

Division of Rheumatology, Allergy, and Immunology, Center for Immunology and Inflammatory Diseases, Massachusetts General Hospital, Harvard Medical School, Boston, Massachusetts, USA.

Tregs control various functions of effector T cells; however, where and how Tregs exert their immunomodulatory effects remain poorly understood. Here we developed a murine model of adoptive T cell therapy and found that Tregs induce a dysfunctional state in tumor-infiltrating CTLs that resembles T cell exhaustion and is characterized by low expression of effector cytokines, inefficient cytotoxic granule release, and coexpression of coinhibitory receptors PD-1 and TIM-3. Induction of CTL dysfunction was an active process, requiring local TCR signals in tumor tissue. Tregs infiltrated tumors only subsequent to Ag-dependent activation and expansion in tumor-draining LNs; however, Tregs also required local Ag reencounter within tumor tissue to induce CTL dysfunction and prevent tumor rejection. Multiphoton intravital microscopy revealed that in contrast to CTLs, Tregs only rarely and briefly interrupted their migration in tumor tissue in an Ag-dependent manner and formed unstable tethering-interactions with $CD11c^+$ APCs, coinciding with a marked reduction of CD80 and CD86 on APCs. Activation of CTLs by Treg-conditioned $CD80/86^{lo}$ DCs promoted enhanced expression of both TIM-3 and PD-1. Based on these data, we propose that Tregs locally change the costimulatory landscape in tumor tissue through transient, Ag-dependent interactions with APCs, thus inducing CTL dysfunction by altering the balance of costimulatory and coinhibitory signals these cells receive.

Introduction

Malignant cellular transformation elicits adaptive immune responses, and growing tumors have usually been selected for their ability to avoid elimination by these responses through a plethora of active and passive mechanisms. Nevertheless, T cells can facilitate rejection of established tumors, both spontaneously and in various settings of cancer immunotherapy. $CD8^+$ CTLs are thought to act through cytotoxic destruction of tumor cells and secretion of effector cytokines. $CD4^+$ T cells provide "help" to the $CD8^+$ CTL response (1–3), but can also have CTL-independent antitumor effects (4, 5). However, most solid malignancies express little or no MHC class II molecules, in contrast to the presence of MHC class I molecules. Therefore, their successful and complete elimination in settings where the immune system is being harnessed to treat tumors in human patients is generally viewed to be dependent on the functions of $CD8^+$ T cells that recognize tumor-specific or tumor-associated Ags (6). For a long time, immunotherapy efforts have therefore been directed at optimizing the induction of $CD8^+$ T cell responses to tumors under the assumption that this may be the rate-limiting step in tumor rejection. More recently, however, it has been recognized that tumor-reactive CTLs are spontaneously generated and can be found in robust numbers both in the bloodstream and in the tumor tissue of patients, but that those cells that have infiltrated the tumors have largely lost their effector functions (7–9). Such tumor-infiltrating CTLs, similar to virus-specific T cells in chronic viral infection, exhibit phenotypic and functional features of T cell exhaustion, such as expression of coinhibitory receptors and impaired secretion of cytokines or cytotoxic proteins (10–12). The importance of these coinhibitory receptors has been emphasized by the recent success of monoclonal antibody therapies to block their function (i.e., immune checkpoint blockade), which have achieved remarkable responses in cancer patients (13, 14). In order to further develop therapeutic approaches that build on the manipulation of coinhibitory pathways, it will be important to understand how the expression of these molecules on T cells is controlled. Also, it would be valuable to know to what extent these immunoregulatory mechanisms affect the outcome of adoptive T cell therapies, which have emerged as an additional promising treatment modality for human cancer patients (15).

$Foxp3^+$ Tregs have been shown to be important contributors to the development of immune tolerance toward tumors, but the mechanisms by which this occurs are still not well understood. They can emerge both from thymic development preferentially through selection on self-Ags (tTreg) and from peripheral conversion of likely predominantly non–self-Ag–specific conventional T cells (pTreg) (16), and both Treg populations have been found in different types of tumors (17, 18). Apart from the Ag specificity of tumor-responsive Tregs, the role that cognate Ag encounter plays in regulating their population dynamics, at both immune induction and effector sites and in eliciting their suppressive effector functions, is still largely unknown. Finally, although a variety of Treg effector mechanisms have been identified (19), the location and the context in which these different mechanisms unfold in vivo has not been well described.

In the present study, we found that tumor-infiltrating Tregs promoted the rapid induction of a state of functional hyporesponsiveness in CTLs that was characterized by impaired cytokine secretion and cytotoxic granule release, as well as coexpression of the coinhibitory receptors PD-1 and TIM-3, hallmarks of what has previously been described as T cell exhaustion in settings of chronic viral infection (20). Using an experimental tumor model that allowed us

Authorship note: Christian A. Bauer and Edward Y. Kim contributed equally to this work.

Conflict of interest: The authors have declared that no conflict of interest exists.

Citation for this article: *J Clin Invest.* 2014;124(6):2425–2440. doi:10.1172/JCI66375.

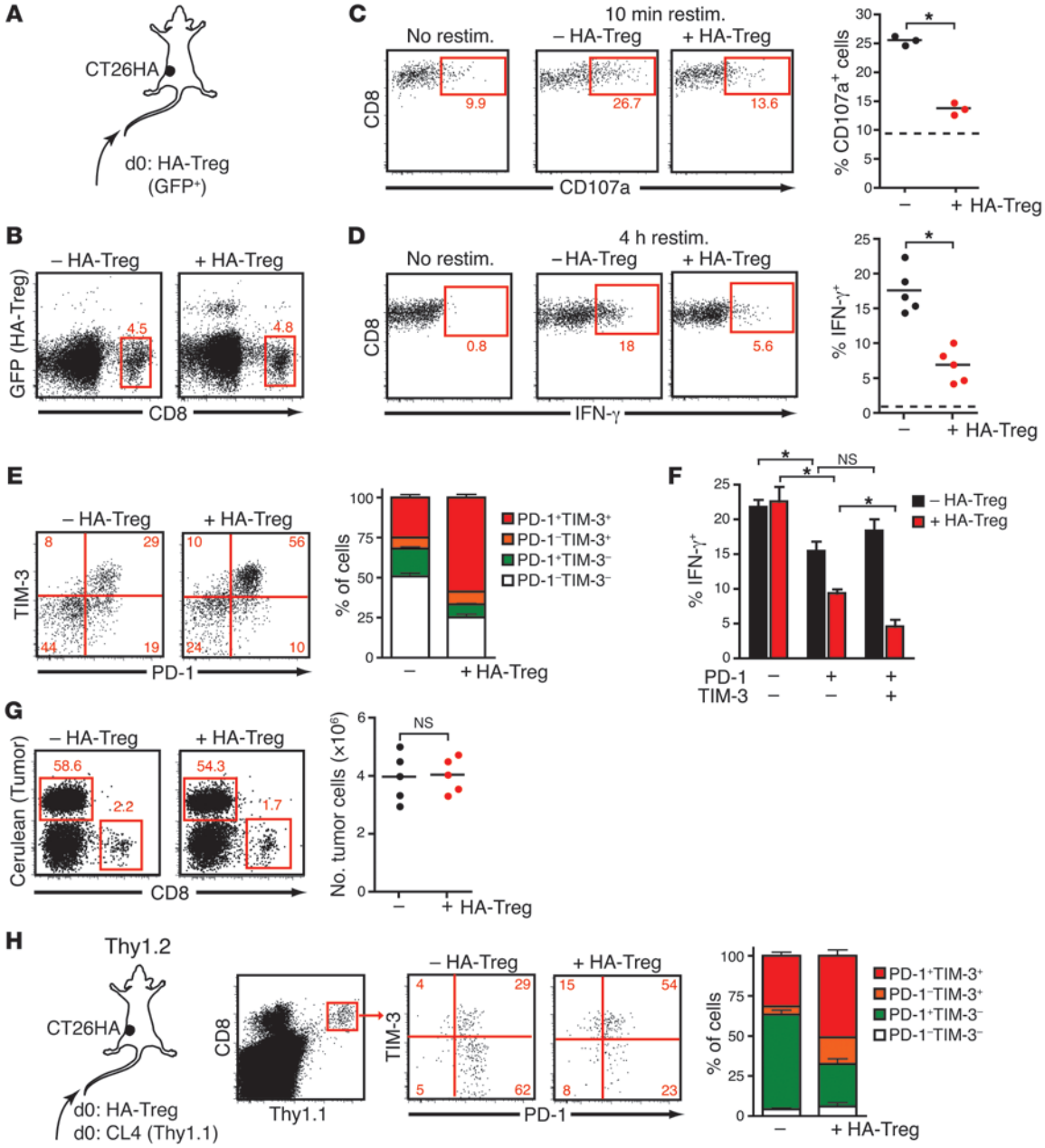

Figure 1

Tumor Ag–specific Tregs aggravate a state of dysfunction of tumor-infiltrating CTLs that resembles exhaustion. (**A**) BALB/c mice were infused with GFP+ HA-Tregs and on the same day implanted in the flank with CT26HA tumors. (**B**–**E**) 9 days later, tumor-infiltrating, host-derived, polyclonal CTLs (**B**) were analyzed for their capacity to degranulate (**C**) and secrete IFN-γ (**D**) ex vivo in response to plate-bound CD3 Abs and for (**E**) expression of PD-1 and TIM-3, compared with CTLs from animals that did not receive HA-Tregs. (**F**) Frequency of cells in the indicated CTL subpopulations expressing IFN-γ upon restimulation. (**G**) Relative frequency of CTLs and CT26HA tumor cells (expressing the fluorescent fusion protein H2B-Cerulean) in day-9 tumors. (**H**) Thy1.2 mice received Thy1.1+ naive, HA-specific CL4 CD8+ T cells together with HA-Tregs, and expression of PD-1 and TIM-3 on tumor-infiltrating CL4 T cells was measured on day 9. Bar graphs in **E** and **H** show relative frequencies of CTLs expressing PD-1, TIM-3, both, or neither. Each experiment shown is representative of at least 2 with similar results; dashed lines in graphs in **C** and **D** indicate background in nonrestimulated CTLs; data represent $n = 3$–5 animals/group. All graphs indicate means; error bars denote SEM (**E**, **F**, and **H**). $^*P < 0.05$.

to track clonal Treg and CTL populations and to independently control their cognate Ag encounter specifically in the tumor tissue, we found that Ag-driven Treg activities in tumor tissue sufficed to induce local CTL dysfunction and to disable tumor rejection, independent of the cells' suppressive activities in tumor-draining LNs (dLNs), where they were initially activated. Induction of dysfunction in differentiated CTLs in tumor tissue proved to be an active process that required TCR signals. Tregs underwent Ag-dependent interactions with CD11c+ tumor APCs and downmodulated their expression of the costimulatory molecules CD80 and CD86 in vivo.

In vitro, this was sufficient to augment the coexpression of TIM-3 and PD-1 on CTLs activated by such Treg-conditioned APCs, while CD28 signaling antagonized their induction upon T cell activation. Our findings suggested that Treg activities in tumor tissue include contact-dependent downregulation of costimulatory molecules on local APCs. The resulting decrease in costimulation delivered to tumor-infiltrating CTLs during Ag re-encounter, which at the same time augments their expression of coinhibitory receptors, culminates in their dysfunction.

Results

Tregs aggravate local functional hyporesponsiveness of tumor-infiltrating CTLs. To investigate the influence of Ag recognition on the population dynamics of Tregs and their ability to regulate effector T cell (Teff) responses against tumors, we sought to develop an experimental system in which we could track clonal populations of Tregs with known specificity for a model Ag. Mice that express both influenza HA as a ubiquitous self-Ag as well as the transgenic T cell receptor TCR-HA, which recognizes the I-E^d–restricted epitope $HA_{107–119}$, generate HA-specific Tregs (referred to herein as HA-Tregs; ref. 21). We enriched LN and spleen cells from these animals for HA-Tregs, which express the transcription factors Foxp3 and Helios and suppress the function of HA-specific $CD4^+$ and $CD8^+$ T cells in vitro (21), and transferred these cells into mice that were subsequently implanted under the skin with HA-expressing CT26 (CT26HA) tumors (Figure 1A and Supplemental Figure 1; supplemental material available online with this article; doi:10.1172/JCI66375DS1). The endogenous T cell response of BALB/c mice against CT26HA tumors is insufficient to facilitate their rejection (22), and we therefore did not expect a change in the rate of tumor growth through HA-Treg–mediated immunoregulatory effects. However, while HA-Tregs did not alter or only mildly reduced the frequency of CTLs in tumor tissue (Figure 1B), we found that HA-Tregs had rendered tumor-infiltrating CTLs hyporesponsive when examining these cells functionally by measuring their ability to degranulate and express IFN-γ in response to short-term TCR triggering (Figure 1, C and D). This functional deficit was paralleled by an increase in their coexpression of the coinhibitory receptors PD-1 and TIM-3 (Figure 1E), which has previously been linked to T cell dysfunction in both mouse and human tumors (10–12). Interestingly, although there was a clear hierarchy of CTL dysfunction in the presence of HA-Tregs, with $TIM\text{-}3^+PD\text{-}1^+$ double-positive cells being least functional, followed by $PD\text{-}1^+$ single-positive cells, this hierarchy was not as pronounced in their absence (Figure 1F). As expected, tumor burden and the ratio of tumor cells to CTLs was not altered in the presence of HA-Tregs at the time of analysis (Figure 1G), which suggests that these differences did not result from a quantitative increase in exposure to tumor Ag.

PD-1 expression has been described as a hallmark of T cell exhaustion in chronic viral infection (20). However, it is also rapidly upregulated in nonexhausted T cells upon activation (23) and may be part of a physiological counterregulatory response that is in place to tune TCR signaling to the amount of available Ag (24). Recent studies in tumors suggest that cells expressing only PD-1 indeed retain Ag responsiveness, while only coexpression of PD-1 and TIM-3 identifies the most profoundly hypofunctional T cells (10, 11). We therefore hypothesized that PD-1 expression by CTLs indicates recent TCR stimulation, but does not by itself report Treg-induced dysfunction. To test this hypothesis, we repeated the above experiment, but also transferred naive CL4 TCR transgenic $CD8^+$ T cells (25), which recognize the H-$2K^d$-restricted $HA_{515–523}$ epitope, before tumor implantation. In the absence of HA-Tregs, but not in their presence, in vivo–primed CL4 T cells rejected CT26HA tumors (Supplemental Figure 2 and ref. 26). Notably, at a time point when tumor burden was not yet different, the fraction of $TIM\text{-}3^+$ cells among $PD\text{-}1^+$ tumor-infiltrating CL4 T cells had more than doubled in the presence of HA-Tregs (from 32% to 70%), while the overall proportion of $PD\text{-}1^+$ cells remained constant. At the same time, the population of cells expressing neither PD-1 nor TIM-3, which represented up to half of the endogenous tumor-infiltrating CTLs, was almost completely absent among CL4 T cells (Figure 1H). Since tumor-infiltrating CTLs derived from the endogenous polyclonal repertoire likely recognize tumor Ags with a broad range of affinities, these data suggested that expression of PD-1 by itself reflects recent Ag recognition with high TCR affinity (as for the CL4 TCR), but only coexpression of PD-1 and TIM-3 is correlated with pronounced T cell dysfunction.

We therefore concluded that Tregs exacerbate the induction of T cell dysfunction in tumor-infiltrating CTLs independent of tumor burden and prevent tumor rejection.

Ex vivo–primed CTLs are subject to local induction of T cell dysfunction through Tregs in a setting of adoptive T cell therapy. We wanted to examine if ex vivo–primed CTLs were also susceptible to Treg-induced dysfunction in a setting that mimics adoptive T cell therapy. We therefore cultured HA peptide–pulsed CL4 splenocytes first with IL-12, then with IL-2, to generate HA-specific CTLs (HA-CTLs; Supplemental Figure 3A). When HA-CTLs were transferred into mice with established CT26HA tumors, they rejected these in an Ag-specific fashion without the requirement to migrate through dLNs for further activation (Supplemental Figure 3, B–D). However, when tumor-bearing mice had previously been seeded with HA-Tregs, HA-CTLs were unable to reject tumors, which grew at a rate comparable to that observed in the absence of any T cell transfer (Figure 2A). In this setting, where a large number of CTLs were injected i.v., HA-Tregs impaired neither the recruitment of CTLs to tumors, nor their infiltration of the tumor parenchyma, within the first 5 days after transfer (Figure 2B and data not shown). We also did not observe a rapid loss of CTL effector differentiation when analyzing the expression of granzyme B or of total (intra- and extracellular) CD107a, which reflect the formation of cytotoxic granules and secretory lysosomes, respectively (Figure 2C). However, as was the case with in vivo–primed CTLs, we observed an inability of tumor-infiltrating HA-CTLs retrieved from HA-Treg–seeded mice 2 days after their adoptive transfer to effectively deploy their lytic cargo when encountering Ag (Figure 2D). Also, a 2- to 3-fold larger fraction of $PD\text{-}1^+$ cells expressed TIM-3 in the presence of HA-Tregs than in their absence (Figure 2E). Equivalent changes were observed for the frequency of CTLs producing neither TNF nor IFN-γ upon restimulation ex vivo (Figure 2F).

Our finding of Treg-mediated induction of T cell dysfunction in this setting of adoptive Teff therapy indicates that while Tregs likely also unfold their immunoregulatory activities already at induction sites of antitumor immune responses, their activity at the effector sites is sufficient to rapidly promote CTL dysfunction.

Only CTLs that encounter their cognate Ag in tumor tissue are susceptible to Treg-induced dysfunction. CTLs may be rendered dysfunctional in tumor tissue because Tregs deprive them of Ag-dependent activation signals required to sustain or fully develop their effector functions. Alternatively, CTLs may receive Ag-dependent inhibitory signals that actively induce their dysfunction. To distinguish between

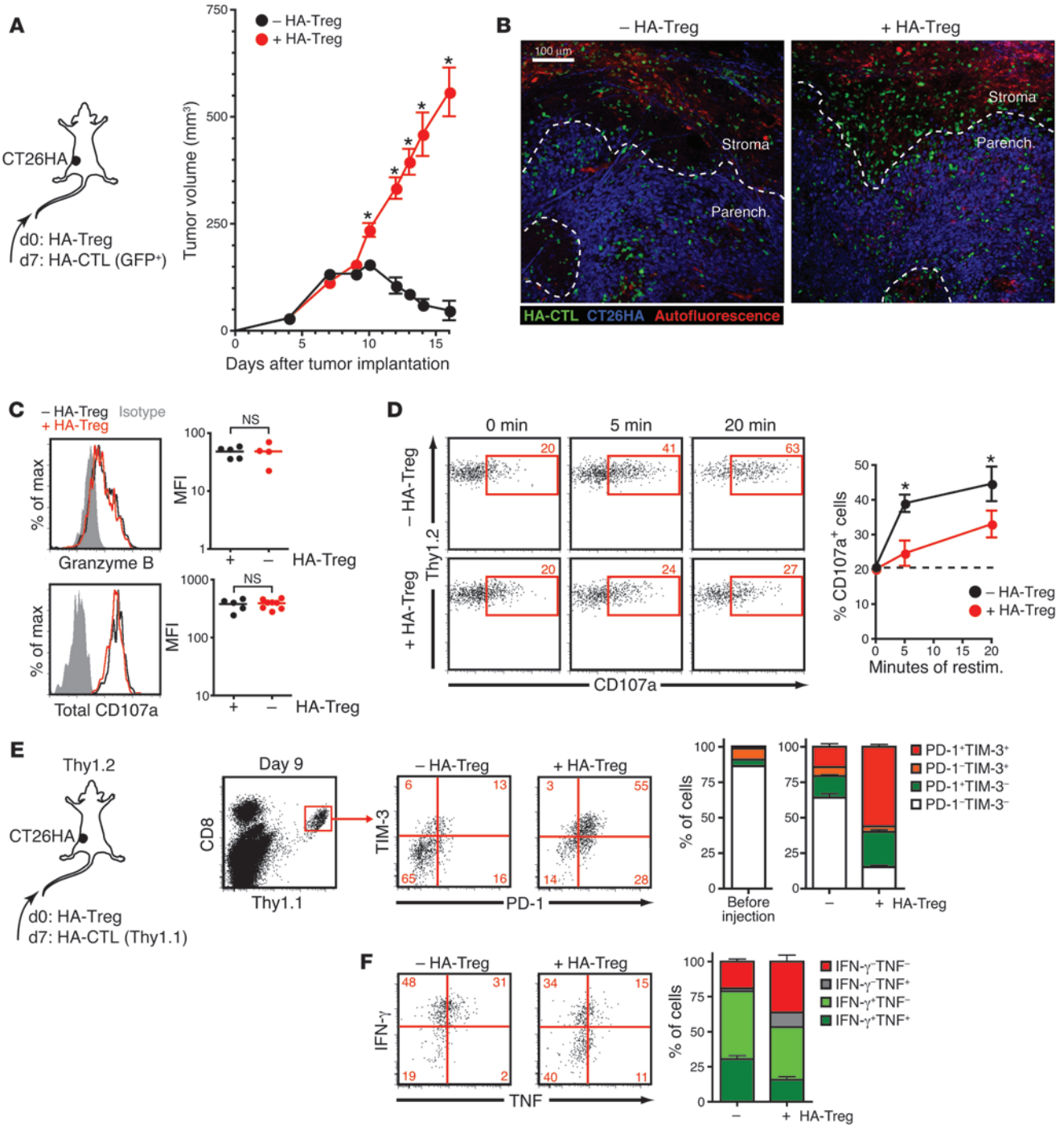

Figure 2

Tregs rapidly amplify CTL dysfunction through local activity in tumor tissue. (**A**) HA-Tregs prevented rejection of established CT26HA tumors by ex vivo–activated HA-CTLs injected at day 7. (**B**) HA-CTLs infiltrate both tumor stroma and parenchyma in presence of HA-Tregs. CT26HA nuclei were marked by expression of the blue fluorescent protein Cerulean fused to histone H2B. Tissue autofluorescence is depicted in red. Scale bar: 100 μm. (**C**) Expression of granzyme B and the lysosomal marker CD107a (intra- and extracellular) in tumor-infiltrating HA-CTLs 3 days after transfer into tumor-bearing mice harboring HA-Tregs or not. (**D**) Impaired degranulation and surface mobilization of CD107a in tumor-infiltrating HA-CTLs 2 days after transfer into animals harboring HA-Tregs. (**E**) Expression of PD-1 and TIM-3 by tumor-infiltrating HA-CTLs. Graph shows the frequency of HA-CTLs expressing PD-1, TIM-3, both, or neither, before and 2 days after transfer into mice harboring HA-Tregs or not. (**F**) Expression of effector cytokines upon short ex vivo restimulation of tumor-infiltrating HA-CTLs. Each experiment shown is representative of 2 (**B**–**F**) or 4 (**A**) with similar results (n = 3–5 per group). All graphs indicate means; error bars denote SEM (**A** and **D**–**F**). *P < 0.05.

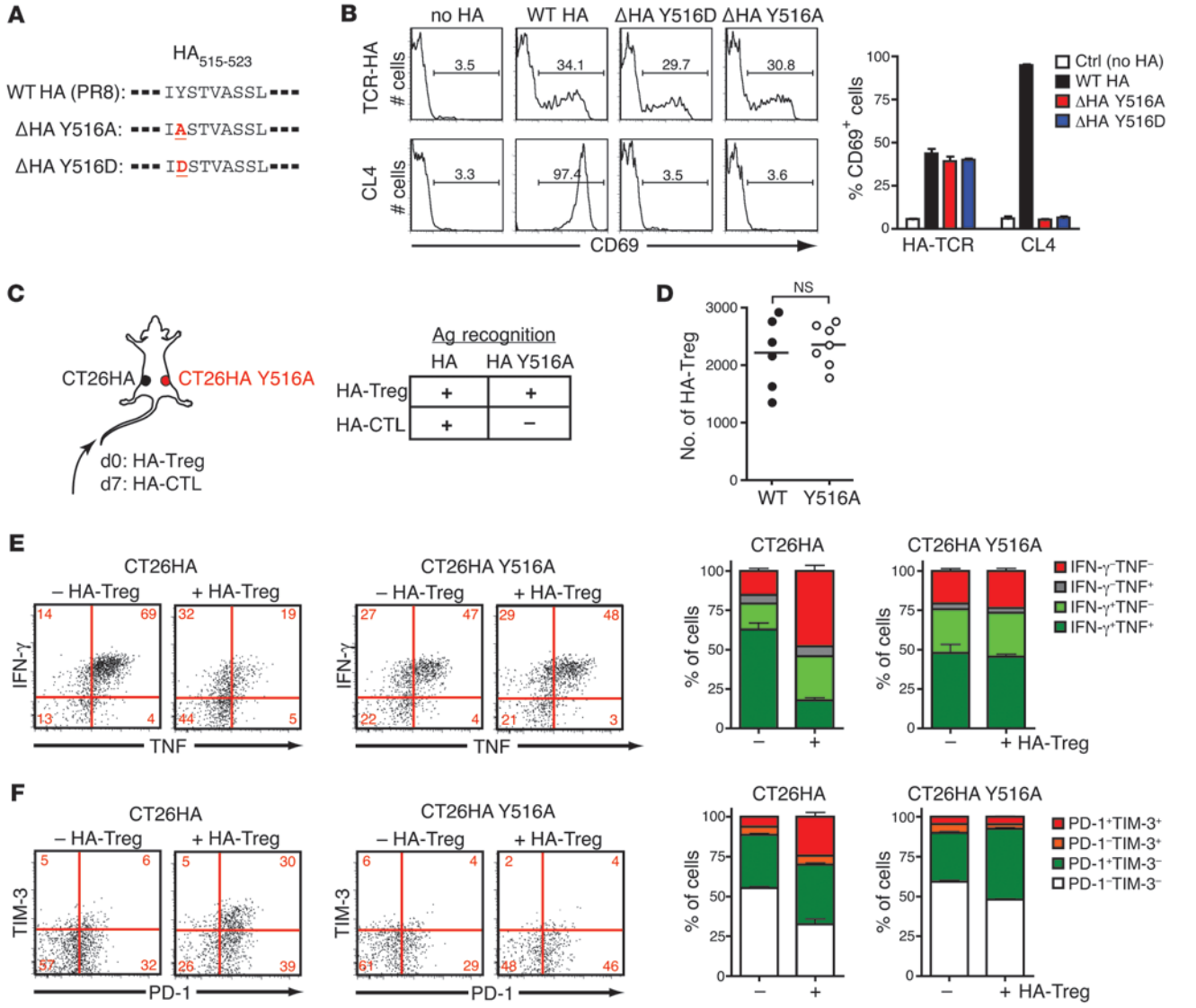

Figure 3

Treg-dependent CTL dysfunction requires their local Ag recognition in tumor tissue. (**A**) The $HA_{515–523}$ determinant of HA was mutated in position 2 to generate HA Y516A and HA Y516D in order to prevent binding to H-2K^d while preserving the $HA_{107–119}$ determinant. (**B**) CT26 cells expressing no HA, WT HA, or either mutant HA were mixed at 1:20 ratios with splenocytes from TCR-HA or CL4 TCR transgenic animals. T cell activation was measured 24 hours later as surface expression of CD69. Graph shows summary of data. Each analysis was performed in triplicate. (**C**) HA-Treg–seeded mice were implanted with both CT26HA and CT26HA Y516A tumors. When 5×10^6 HA-CTLs were injected at day 7, they would recognize HA only in CT26HA tumors, not CT26HA Y516A tumors, while HA-Tregs would encounter "their" HA determinant in both. (**D**) Similar HA-Treg recruitment in CT26HA and CT26HA Y516A tumors on day 11 after tumor implantation. (**E**) Expression of effector cytokines upon ex vivo restimulation of HA-CTLs from WT or mutant tumors retrieved 4 days after adoptive transfer into animals seeded with HA-Tregs or not. Graphs show fractions of CTLs expressing IFN-γ, TNF, both, or neither. (**F**) Expression of PD-1 and TIM-3 by HA-CTLs from WT or mutant tumors of animals harboring HA-Tregs or not. Graphs show fractions of CTLs expressing PD-1, TIM-3, both, or neither. Each experiment in **C**–**F** is representative of 2 (n = 3–4 per group) with similar results. All graphs indicate means; error bars denote SD (**B**) or SEM (**D**–**F**).

these possibilities, we sought to create conditions in tumor tissue under which Ag recognition by HA-CTLs, but not HA-Tregs, is selectively disabled. We therefore mutated the $HA_{515–523}$ determinant recognized by the CL4 TCR to abrogate presentation by MHC I in BALB/c mice (Figure 3A). This prevented in vitro activation of CL4, but not of TCR-HA transgenic T cells by mutant HA (either Y516A or Y516D) expressed in CT26 cells (Figure 3B). We then implanted HA-Treg–seeded mice with CT26HA tumors in one flank and CT26HA Y516A tumors in the other, and transferred HA-CTLs 7 days later (Figure 3C). Accumulation of HA-Tregs in tumor tissue was not altered by the HA mutation (Figure 3D). Since HA-CTLs did not recognize the mutant HA determinant, they were not expected to reject CT26HA Y516A tumors, regardless of whether they were functionally suppressed by HA-Tregs. We therefore analyzed their capacity for effector cytokine secretion upon restimulation ex vivo as a measure of their functional

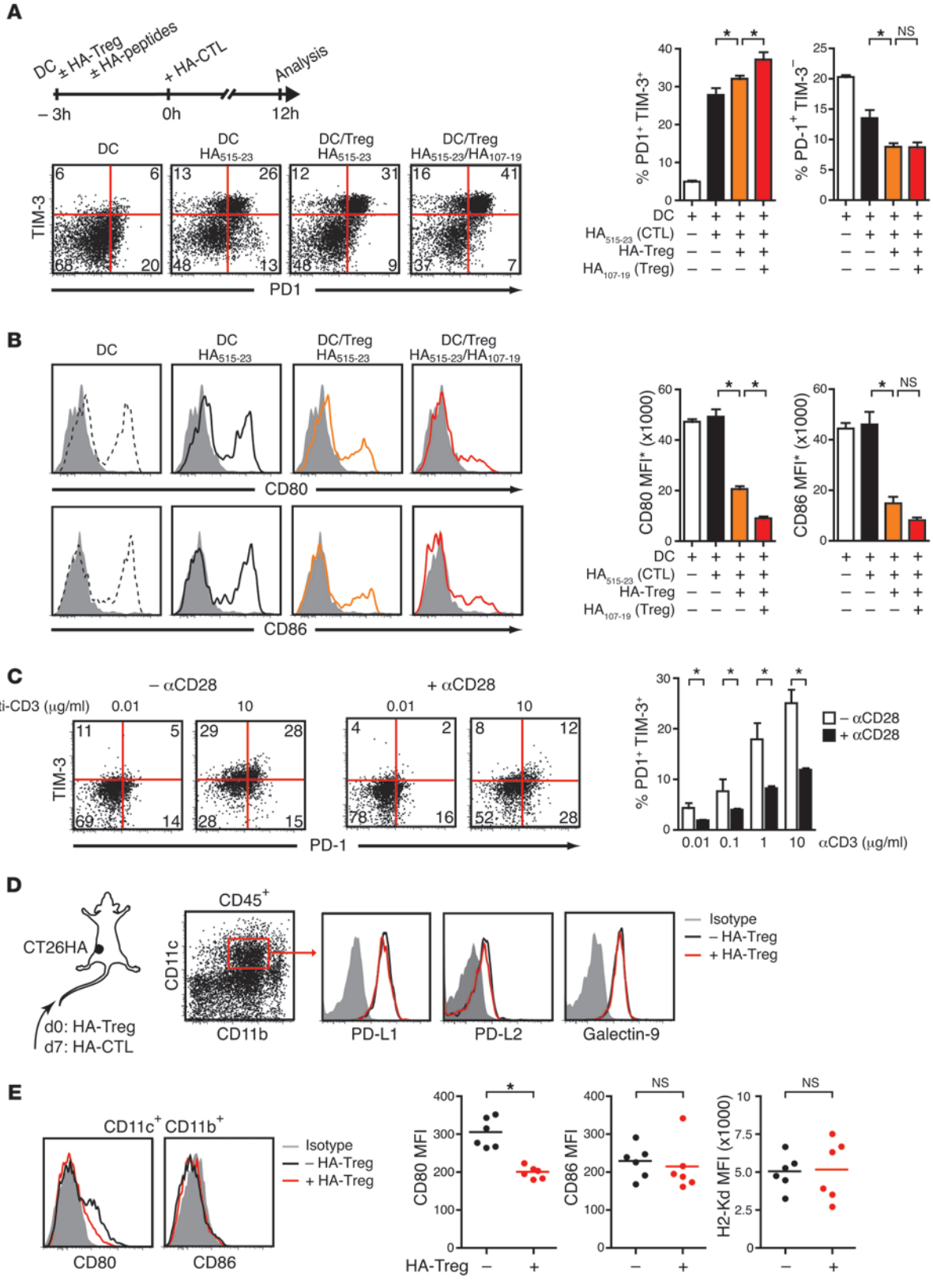
A
DC ± HA-Treg ± HA-peptides
+ HA-CTL
Analysis
– 3h
0h
12h
DC
DC HA515-23
DC/Treg HA515-23
DC/Treg HA515-23/HA107-19
TIM-3
PD1
6 6 68 20
13 26 48 13
12 31 48 9
16 41 37 7
% PD1+ TIM-3+
% PD-1+ TIM-3–
DC
HA515-23 (CTL)
HA-Treg
HA107-19 (Treg)
B
CD80
CD86
CD80 MFI* (x1000)
CD86 MFI* (x1000)
C
– αCD28
+ αCD28
Anti-CD3 (μg/ml) 0.01 10
11 5 69 14
29 28 28 15
4 2 78 16
8 12 52 28
PD-1
% PD1+ TIM-3+
0.01 0.1 1 10 αCD3 (μg/ml)
D
CT26HA
d0: HA-Treg
d7: HA-CTL
CD45+
CD11c
CD11b
PD-L1
PD-L2
Galectin-9
Isotype
– HA-Treg
+ HA-Treg
E
CD11c+ CD11b+
CD80
CD86
CD80 MFI
CD86 MFI
H2-Kd MFI (x1000)
HA-Treg
NS

Figure 4
Tregs condition DCs to reduce their costimulatory activity and augment coexpression of PD-1 and TIM-3 by CTLs. (**A**) LPS-activated splenic DCs were either not pulsed or pulsed with $HA_{515–523}$ peptide, $HA_{107–119}$ pepitde, or both and cocultured with HA-Tregs for 3 hours before addition of HA-CTLs, followed by analysis for expression of PD-1 and TIM-3 on CTLs 12 hours later. (**B**) As in **A**, but DCs were analyzed for expression of CD80 and CD86 directly before addition of CTLs. (**C**) HA-CTLs were reactivated for 3 hours by the indicated doses of anti-CD3ε antibodies in the absence or presence of activating anti-CD28 antibodies and analyzed for expression of PD-1 and TIM-3. (**D**) 10-day-old CT26HA tumors seeded with HA-Tregs or not were analyzed for expression of PD-L1, PD-L2, and galectin-9 on $CD11b^+CD11c^+$ DCs. (**E**) Expression of CD80 and CD86 on $CD11b^+CD11c^+$ DCs from 10-day-old CT26HA tumors harboring HA-Tregs or not. Each experiment shown is representative of at least 2 (n = 5 each) with similar results. Filled histograms show isotype staining. All graphs indicate means; error bars denote SD (**A**–**C**) or SEM (**E**). *$P < 0.05$.

responsiveness. In tumors expressing WT HA, almost 3 times as many HA-CTLs expressed neither IFN-γ nor TNF, whereas 3 times fewer cells expressed both cytokines, in the presence of HA-Tregs. However, in tumors where only HA-Tregs, but not HA-CTLs, recognized their cognate Ag, we observed no change in the cytokine expression capacity of CTLs in the presence of Tregs, which resembled that of functional CTLs in WT tumors in the absence of HA-Tregs (Figure 3E). Analogously, the fraction of CTLs coexpressing PD-1 and TIM-3 tripled in CT26HA tumors, but remained constant in CT26HA Y516A tumors, in the presence of HA-Tregs compared with their absence (Figure 3F). Hence, under the local influence of Tregs, primed CTLs are rendered dysfunctional at effector sites through encounters with APCs presenting their cognate Ag, which indicates that the dysfunctional state is actively induced.

Treg-conditioned DCs induce coexpression of PD-1 and TIM-3 by CTLs. How could Tregs facilitate enhanced coexpression of PD-1 and TIM-3 and concomitant CTL dysfunction? Since only CTLs that encounter their cognate Ag in tumor tissue are susceptible to Treg-mediated effects, we hypothesized that Tregs may functionally modify tumor-infiltrating DCs or other APCs, leading to an altered form of T cell activation culminating in dysfunction. To test this hypothesis in a simplified in vitro system, we cocultured HA-Tregs with LPS-activated splenic DCs, and 3 hours later added HA-CTLs to this culture. Interestingly, $HA_{515–523}$ peptide–pulsed DCs alone induced coexpression of PD-1 and TIM-3 in HA-CTLs, which expressed low amounts of PD-1 at baseline. However, preconditioning of DCs with HA-Tregs further increased the frequency of double-positive CTLs, an effect that was most pronounced when DCs were pulsed with the $HA_{107–119}$ peptide recognized by the HA-Treg TCR (Figure 4A). Hence, HA-Tregs change DCs functionally, and most effectively in the context of Ag-dependent interactions, in ways that increase the subsequent Ag-dependent coinduction of PD-1 and TIM-3 on HA-CTLs activated by these DCs.

One of the core mechanisms of Treg-mediated immunoregulation is downregulation of the costimulatory molecules CD80 and CD86 on DCs via CTLA-4–mediated transendocytosis (27, 28). Indeed, when we analyzed HA-Treg–conditioned DCs, we noticed a rapid and dramatic decrease in CD80 and CD86 expression, which was again most pronounced in DCs presenting cognate Ag to Tregs (Figure 4B). This suggests that a paucity of costimulatory ligands on DCs may enhance coinduction of PD-1 and TIM-3 in CTLs through TCR activation. To directly test whether costimulation in CTLs could regulate PD-1 and TIM-3 coinduction, we activated HA-CTLs with anti-CD3 antibodies in the presence or absence of agonistic antibodies binding the costimulatory receptor CD28 and found that costimulation indeed repressed the simultaneous induction of PD-1 and TIM-3 (Figure 4C). Therefore, cosignaling can control the expression of coinhibitory molecules in differentiated CTLs.

To explore the potential relevance of this mechanism to the suppression of HA-CTLs in HA-Treg–infiltrated tumors, we analyzed $CD11b^+CD11c^+$ DCs from CT26HA tumors for ligands of various cosignaling molecules. HA-Tregs did not alter the robustly expressed coinhibitory PD-1 and TIM-3 ligands PD-L1, PD-L2, and galectin-9 on DCs or on other tumor APCs (Figure 4D and Supplemental Figure 4), in line with previous in vitro studies (29). Expression of CD80 and CD86, in contrast, was low to begin with, likely reflecting poor innate immune activation of DCs in tumor tissue as well as the activity of endogenous Tregs, but HA-Tregs further decreased residual CD80 on DCs to near-background levels (Figure 4E), thereby depriving tumor-infiltrating CTLs of potential costimulatory signals.

Collectively, these observations suggest that Tregs facilitate CTL dysfunction in tumor tissue through local downregulation of costimulatory molecules on DCs, which in turn activate CTLs in a fashion that culminates in dysfunction.

Ag-dependent population dynamics of HA-Tregs in tumor tissue and dLNs. In order to further explore the requirements for HA-Tregs to induce T cell dysfunction in HA-CTLs, we first wanted to understand their population dynamics in response to growing tumors. When we implanted animals with both CT26HA and CT26 tumors, HA-Tregs accumulated only in dLNs of the former (Figure 5A), suggestive of Ag-dependent local activation and clonal expansion. Indeed, HA-Tregs diluted the proliferation marker CFSE concomitantly with upregulation of the activation markers CD44 and CD69 (Figure 5B). HA-Tregs in dLNs of CT26 tumors were either undivided or had divided more than 4 times, which suggests that they initiated proliferation elsewhere and subsequently migrated to this location. Moreover, no divided HA-Tregs were found in dLNs of CT26 tumors in animals without contralateral implantation of a CT26HA tumor (data not shown). Finally, unlike their counterparts in CT26HA dLNs, HA-Tregs in CT26 dLNs did not express CD69 on their cell surface (Figure 5B), indicative of a lack of recent Ag encounter that could drive proliferation.

Despite continuing tumor growth, HA-Treg numbers in CT26HA dLNs declined after peaking at day 7 (Figure 5A). In contrast, they first appeared in appreciable numbers in tumors at this time (Figure 5C). Here, similar to dLNs, HA-Tregs were found in much greater numbers in HA-expressing tumors, which suggests that local encounters with APCs presenting their cognate Ag are also important for their accumulation at effector sites.

While these observations supported the notion that Tregs require Ag-dependent activation and expansion in dLNs before accumulation in tumors, they could also be explained by the need for tumors to reach a certain size and develop robust vascularization before permitting Treg recruitment, independent of expansion in dLNs. To distinguish between these possibilities, we transferred 2 differentially marked populations of HA-Tregs, before and 3 days after tumor implantation. On day 7, comparable numbers of HA-Tregs derived from each population were found in dLNs, spleen, and nondraining LNs, albeit in low numbers at the latter 2 sites. At the same time, HA-Tregs from the second transfer had

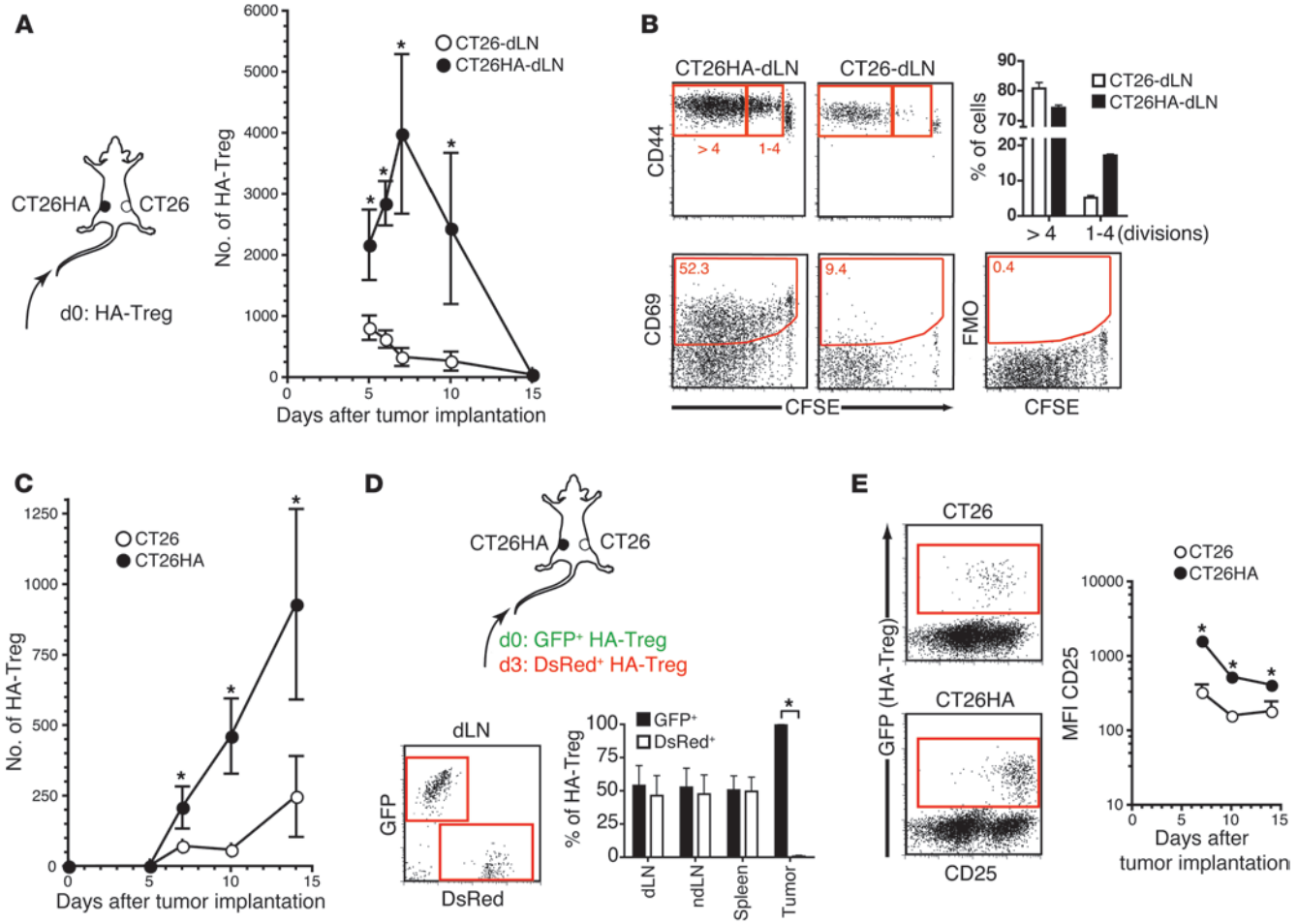

Figure 5

Ag-dependent Treg dynamics in tumor tissue and dLNs. (**A**) BALB/c mice were infused with GFP+ HA-Tregs and on the same day implanted in each flank with CT26HA and CT26 tumors. Inguinal dLNs were harvested from groups of 2–3 animals on various days after tumor implantation to analyze the number of HA-Tregs. (**B**) CFSE-labeled HA-Tregs in LNs were analyzed for proliferation and expression of activation markers CD44 and CD69 4 days after tumor implantation. Graph shows proportion of cells that had divided 1–4 and >4 times. FMO, fluorescence minus one control. (**C**) Tumors were harvested from groups of 2–3 animals on various days after tumor implantation to analyze the number of HA-Tregs. (**D**) As in **A** and **C**, but Thy1.1+ animals received a second infusion of DsRed-expressing HA-Tregs on day 3. Dot plot shows Thy1.2+ HA-Tregs in CT26HA dLNs on day 7. Graph shows proportion of HA-Tregs from first (GFP+) and second (DsRed+) infusion in dLNs, nondraining LNs (ndLN), spleen, and CT26HA tumors on day 7. (**E**) Expression of CD25 on HA-Tregs analyzed in **C**. Dot plots show results from day 7. Graph shows MFI of GFP+ HA-Tregs. Each experiment shown is representative of 2 (n = 3 per group) with similar results. All graphs indicate means; error bars denote SEM. *P < 0.05.

not yet begun to infiltrate tumors (Figure 5D). This does not rule out the possibility that Tregs have the capacity in some settings to directly migrate to effector sites without prior activation in LNs (30). However, it does indicate that accumulation at effector sites subsequent to induction sites does not reflect delayed competence of the growing tumors compared with LNs to support Treg recruitment, but rather that Treg activation and expansion in dLNs precedes their migration to tumors.

Upon recruitment of activated HA-Tregs to effector sites, their local accumulation may rely on continued Ag-dependent proliferation and survival. Treg survival at effector sites has been suggested to depend on signals through the costimulatory receptor inducible costimulator (ICOS; ref. 31) or IL-2 released by Teffs (32). The capacity to receive IL-2 signals requires the high-affinity IL-2 receptor α-chain CD25. High-level expression of CD25 by Tregs, in turn, depends on continuous TCR signaling (33–35). Poor HA-Treg accumulation in CT26 tumors may therefore follow downregulation of CD25 in the absence of Ag encounter, and result in reduced competitive survival fitness. In line with this hypothesis, we found that while CD25 expression by HA-Tregs declined over time in all tumors, HA-Tregs retrieved from CT26 tumors consistently expressed up to 5-fold less CD25 than did those from CT26HA tumors (Figure 5E). Endogenous Tregs, on the other hand, likely responding to unidentified Ags in the tumor environment, expressed similar levels of CD25 in both CT26 and CT26HA (data not shown).

Local Ag encounter by Tregs at effector sites is required for suppression of CTL effector function. The Ag-dependent accumulation of HA-Tregs observed in tumor tissue suggested, but did not formally prove, that their local presence there is required to prevent tumor rejec-

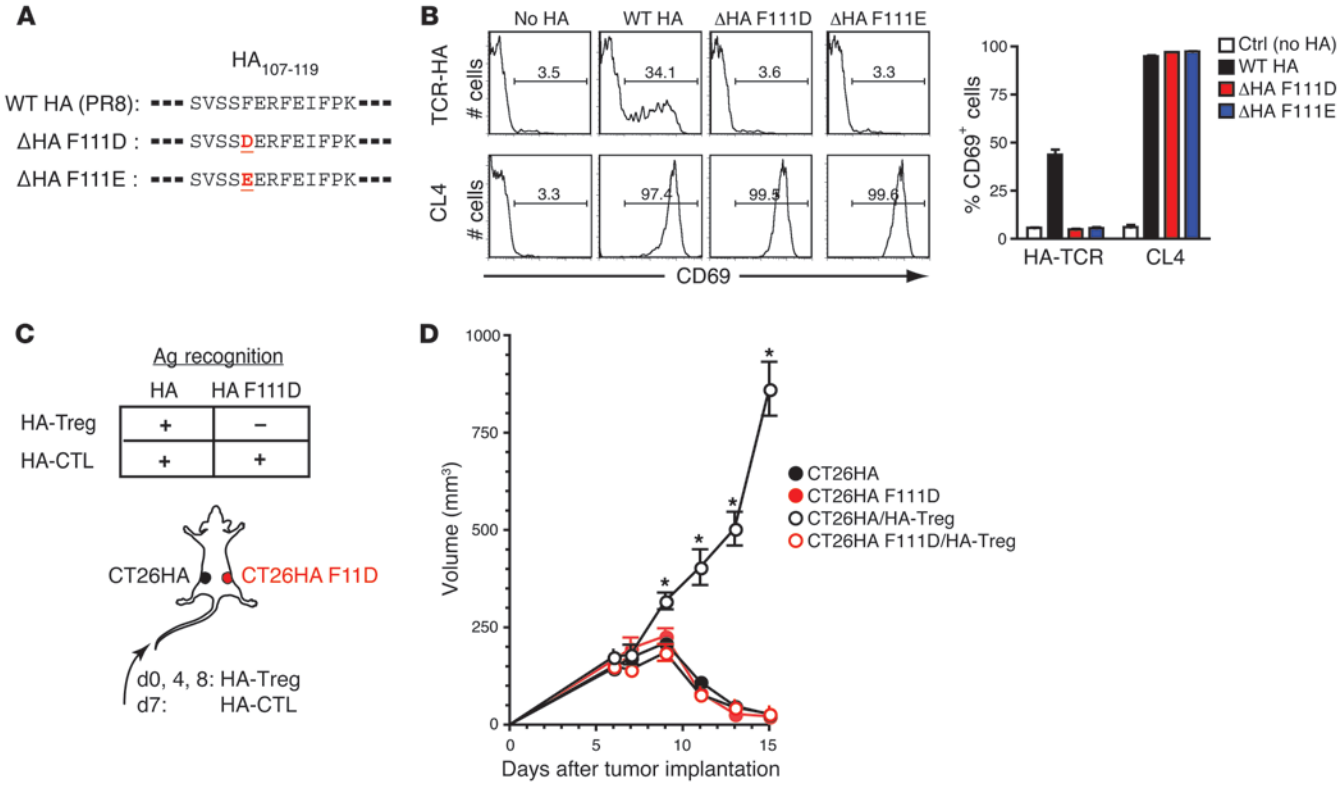

Figure 6

Treg-mediated inhibition of tumor rejection requires local Ag recognition in tumor tissue. (**A**) The $HA_{107–119}$ determinant of HA was mutated in position 5 to generate HA F111D and HA F111E in order to prevent epitope binding to I-E^d while preserving the $HA_{515–523}$ determinant. (**B**) CT26 cells expressing either no HA, WT HA, or either mutant HA were mixed at 1:20 ratios with splenocytes from TCR-HA or CL4 TCR transgenic animals. T cell activation was measured 24 hours later as surface expression of CD69. Each analysis was performed in triplicate; graph shows summary of data. (**C**) Mice implanted with both CT26HA and CT26HA F111D tumors were repetitively injected with HA-Tregs on days 0, 4, and 8. HA-Tregs only expanded in CT26HA dLNs, but subsequently, after entry into the bloodstream, had access to both CT26HA and CT26HA F111D tumors. However, they would only re-encounter their cognate Ag in CT26HA tumors. (**D**) When 5×10^6 HA-CTLs were injected on day 7, HA-Tregs controlled HA-CTL–mediated rejection of CT26HA tumors, but not CT26HA F111D tumors. Data represent 3 mice per group in 1 representative of 2 independent experiments performed. All graphs indicate means; error bars denote SD (**B**) or SEM (**D**). *$P < 0.05$ vs. all other groups.

tion by HA-CTLs. We therefore sought to create conditions under which adoptively transferred HA-CTLs locally recognize their cognate Ag in tumor tissue, enabling tumor rejection, while HA-Tregs that first expand in dLNs do not re-encounter their Ag once they enter tumor tissue. We generated HA mutants in which the I-E^d–restricted HA determinant recognized by the transgenic TCR-HA receptor does not bind to MHC II in BALB/c mice (Figure 6A). When CT26 tumor cells expressing these HA mutants were mixed with splenocytes, transgenic $CD4^+$ T cells expressing the TCR-HA receptor were not activated, while activation of $CD8^+$ CL4 T cells was intact (Figure 6B). When we implanted mice with CT26HA tumors (expressing WT HA) in one flank and tumors expressing the CT26HA F111D mutant in the other, HA-Tregs were expected to be activated only in CT26HA dLNs, but upon LN egress have equal access via the bloodstream to both CT26HA and CT26HA F111D tumors. However, they would only re-encounter their cognate Ag in CT26HA tumors, not in CT26HA F111D tumors, while adoptively transferred HA-CTLs would recognize their preserved HA determinant in either tumor (Figure 6C). Strikingly, we found that even in mice that had received several injections of HA-Tregs, CT26HA F111D tumors were rejected, whereas CT26HA tumors in the same animals were tolerated (Figure 6D). Thus, the capacity of HA-Tregs to control tumor rejection was fully dependent on their ability to locally recognize their cognate Ag at the effector site.

Dynamics of Treg interactions with APCs in tumor tissue. CT26 tumor cells are of epithelial origin, and did not detectably express cell surface MHC II molecules in vitro and only minimal amounts in vivo (data not shown). It is therefore likely that most presentation of tumor cell–derived HA to tumor-infiltrating HA-Tregs occurs on other nonhematopoietic or on hematopoietic APCs. To study the dynamics of these interactions, we seeded mice with GFP^+ HA-Tregs before implantation of CT26HA tumors in the scruff of the neck and either CT26HA or CT26 tumors into dorsal skinfold chambers (DSFCs), as described previously (36). Multiphoton intravital microscopy (MP-IVM) analysis of DSFC tumors 9 days later showed that HA-Tregs had populated both the tumor parenchyma and the surrounding tumor stroma (Figure 7A and Supplemental Videos 1–4). The majority of cells migrated at high speeds in both compartments. In CT26HA tumors, but not in CT26 control tumors, HA-Treg migration was interrupted by brief periods of low motility (Figure 7C), suggesting transient Ag-dependent stabilization of APC contacts. This was in stark contrast to the

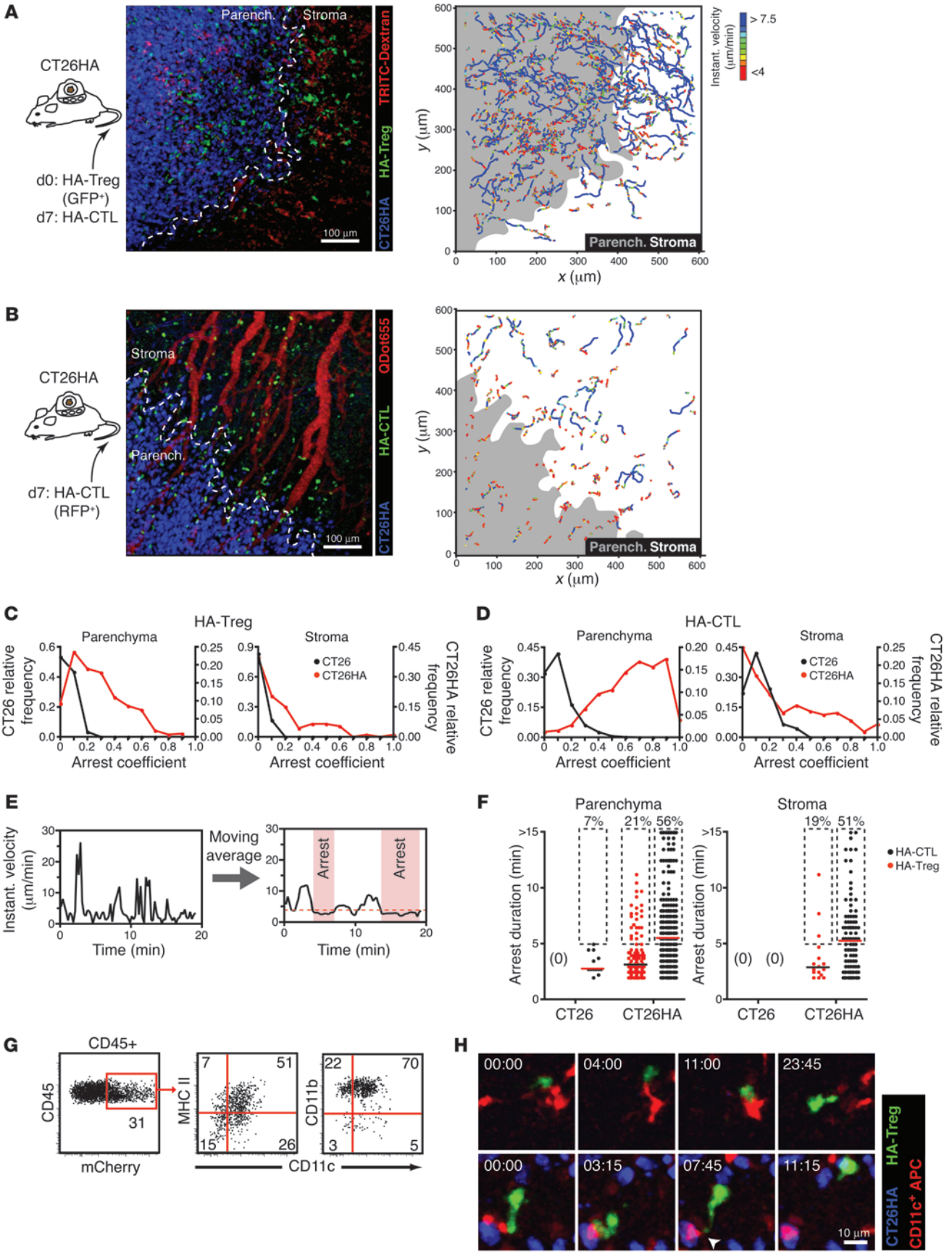
A
CT26HA
d0: HA-Treg (GFP+)
d7: HA-CTL
Parench.
Stroma
100 μm
TRITC-Dextran
HA-Treg
CT26HA
Instant. velocity (μm/min)
> 7.5
<4
y (μm)
x (μm)
Parench. Stroma
B
CT26HA
d7: HA-CTL (RFP+)
Stroma
Parench.
100 μm
QDot655
HA-CTL
CT26HA
C
HA-Treg
Parenchyma
Stroma
CT26
CT26HA
CT26 relative frequency
CT26HA relative frequency
Arrest coefficient
D
HA-CTL
E
Instant. velocity (μm/min)
Moving average
Arrest
Time (min)
F
Parenchyma
Stroma
7%
21%
56%
19%
51%
Arrest duration (min)
HA-CTL
HA-Treg
(0)
CT26
CT26HA
G
CD45+
CD45
mCherry
31
MHC II
CD11b
CD11c
7
51
15
26
22
70
3
5
H
00:00
04:00
11:00
23:45
03:15
07:45
11:15
10 μm
HA-Treg
CD11c+ APC

Figure 7
Tregs only transiently stabilize APC contacts in tumor parenchyma and stroma. (**A**) DSFCs were installed on BALB/c mice; 2 days later, H2B-Cerulean–expressing CT26HA tumors were implanted into the chambers, and animals were infused with GFP$^+$ HA-Tregs. On day 7, mice were injected with (unlabeled) HA-CTLs; 2 days later, HA-Treg behavior was recorded by MP-IVM. Micrograph shows HA-Tregs (green) at the border between tumor parenchyma (blue) and stroma 2 hours after injection of 150 kDa TRITC-Dextran, which was taken up by tumor-resident phagocytes (red). Right: Tracks of HA-Tregs with color-coded instantaneous velocity. (**B**) Similar to **A**, but no HA-Tregs were injected, and HA-CTLs expressed H2B-mRFP (green). Mice were i.v. injected with quantum dots to label the tumor vasculature (red). (**C** and **D**) Histograms of arrest coefficients of HA-Tregs (**C**) and HA-CTLs (**D**) in the tumor parenchyma and stroma of CT26 and CT26HA tumors. (**E**) Migratory tracks were smoothed through a moving average, and segments of continuous average motility <4 μm/min lasting >2 minutes were scored as arrests. (**F**) Duration of HA-Treg and HA-CTL arrests and frequency of arrests >5 minutes (boxed regions) in tumor parenchyma and stroma of CT26 and CT26HA tumors. Lines indicate medians. (**G**) Phenotype of CD45$^+$ mCherry$^+$ cells from CT26HA tumors. (**H**) 2 examples (of >20 observed) of HA-Tregs (green) interacting with CD11c-mCherry$^+$ APCs (red) in a CT26HA tumor. Arrowhead indicates site of characteristic Treg tethering upon disengagement from APCs. Time shown in min:s. Data in **C**, **D**, and **F** are pooled from 5–8 individual recordings of different ROIs from 2–3 independent experiments per group. Data in **G** and **H** are from 2 independent experiments. Scale bars: 100 μm (**A** and **B**); 10 μm (**H**).

behavior of HA-CTLs adoptively transferred 2 days earlier, which showed pronounced Ag-dependent stopping in the parenchyma of CT26HA tumors, but even in the stroma arrested more frequently than HA-Tregs (Figure 7, B and D, and Supplemental Video 5). To investigate the stability of presumptive HA-Treg and HA-CTL contacts with APCs causing their arrest, we analyzed the duration of intervals during which cells continuously moved at an instantaneous velocity of <4 μm/min (Figure 7E). While the majority of HA-Treg arrests lasted less than 5 minutes, both in stroma and in parenchyma, most HA-CTL arrests were longer than 5 minutes and in the parenchyma often exceeded 10 minutes (HA-CTL, 13%; HA-Treg, 2%; Figure 7F).

Migratory arrests by HA-Tregs occurred preferentially directly adjacent to accumulations of i.v. injected and extravasated dextran (Supplemental Video 4), presumably reflecting interactions with phagocytic APCs that had taken up both extracellular dextran as well as tumor-derived Ag. In contrast, HA-Treg migration was unrestricted in areas of low dextran uptake. To more specifically reveal the identity of APCs that interacted with HA-Tregs in tumor tissue, we crossed BALB/c mice with CD11c-mCherry transgenic animals (37), implanted CT26HA tumors into the F1 offspring, and transferred HA-Tregs. Red fluorescent cells in tumor tissue were mostly CD11c$^+$CD11b$^+$MHC II^{hi} (Figure 7G). Using MP-IVM, we found that HA-Treg migratory pauses consistently occurred during interactions with mCherry$^+$ APCs (Figure 7H and Supplemental Video 6). However, these interactions were rather dynamic and did not lead to the stable arrest behavior previously observed for Tregs interacting with DCs in LNs in the context of autoimmune diabetes (38). Upon disengaging, HA-Tregs often remained tethered to APCs via their uropods before ultimately detaching. Together, our observations on Treg behavior in tumors suggest that encounters with APCs presenting their cognate Ag promote adhesive interactions, but not stable migratory arrest.

Since in some contexts, Treg suppression of Teffs can be contact dependent (39), we wanted to test whether HA-Tregs and HA-CTLs interact directly with each other in tumor tissue. We therefore performed MP-IVM experiments in which both HA-Tregs and HA-CTLs were visualized (Figure 8, A and B, and Supplemental Videos 7 and 8). In agreement with the results of previous static imaging studies in human tumors (7), we occasionally observed prolonged colocalization of HA-Tregs and HA-CTLs (Figure 8B and Supplemental Video 8). However, in our dynamic recordings, we did not observe these cells to form interfaces suggestive of direct physical contact. Alternatively, simultaneous interactions with shared APCs may cause such colocalization events. Testing this hypothesis will require visualization of candidate APCs in future studies.

These findings led us to conclude that Tregs are able to utilize brief and unstable APC encounters in order to receive the TCR signals that facilitate their accumulation in tumor tissue, to locally downregulate costimulatory molecules on DCs, and to suppress the cytotoxic antitumor T cell response.

Discussion

In this study, we showed for the first time that Tregs recognizing their cognate Ag in tumor tissue amplify a local immunoregulatory process that induced in tumor-infiltrating CTLs a state of functional hyporesponsiveness characterized by coexpression of the coinhibitory receptors TIM-3 and PD-1, and that sufficed to prevent tumor rejection. An experimental system that was designed to mimic aspects of adoptive T cell therapy in cancer patients allowed us to determine that the Ag-dependent activities of Tregs in the tumor tissue were sufficient to induce CTL dysfunction and prevent CTL-dependent tumor rejection, independent of effects exerted in dLNs. By selectively controlling local Ag presentation to both Tregs as well as the CTLs that they regulate, we identified a role for Ag recognition by both cell types in determining their local population dynamics and functional interplay at effector sites. Using intravital microscopy, we found that in contrast to CTLs, Tregs only very transiently stabilized their cognate interactions with APCs, which were nevertheless critical for their accumulation in tumor tissue and their ability to prevent tumor rejection. Ag recognition by CTLs, conversely, was required not only for the rejection of tumors, but also for the rapid acquisition of a state of functional hyporesponsiveness that was amplified under the influence of Tregs.

The origin and Ag specificity of Tregs that inhibit T cell responses against tumors is still under investigation, and may depend on tissue origin and location of the malignancy (17, 18). Some tumors are infiltrated by both pTregs and tTregs, as distinguished by the expression of neuropilin-1 (17). Since tTregs preferentially express self-reactive TCRs (40–45), those found in tumor tissue likely respond to tumor-associated self-Ags or normal tissue self-Ags (46), whereas tumor-reactive pTregs may derive from tumor neoantigen–specific Foxp3$^-$CD4$^+$ T cells.

CD44^{hi} memory-phenotype Tregs preferentially accumulate in LNs that drain tissues where their cognate self-Ag is expressed (47), which suggests that local Ag encounter induces an intermediate state of Treg activation in the steady state. It is from this population of preactivated Tregs that, in a genetic mouse breast cancer model, tumor-reactive Tregs were shown to derive. In addition to TCR signals, these cells required unidentified tumor-induced factors in order to accelerate their proliferation and expand in dLNs (48). These tumor-induced factors could include TNF (49), but

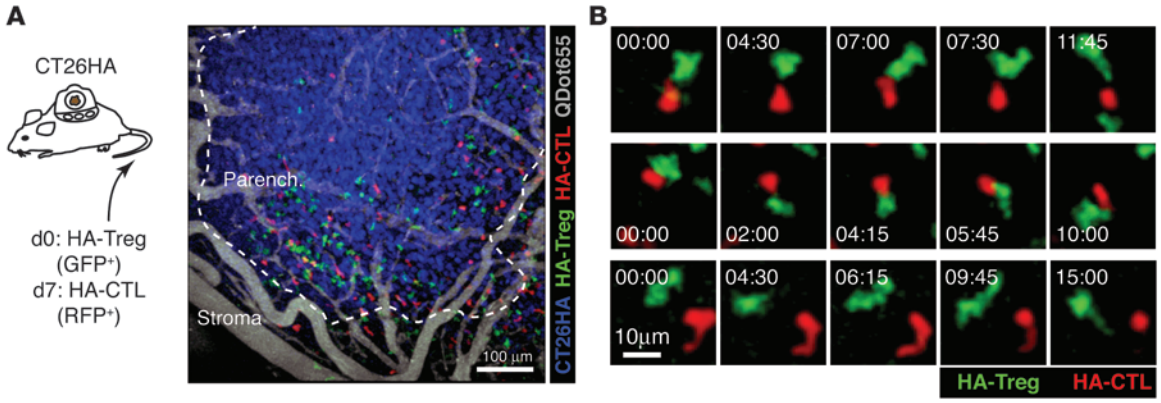

Figure 8

HA-Tregs and HA-CTLs colocalize, but do not directly interact, in tumor tissue. DSFCs were installed on BALB/c mice; 2 days later, histone H2B-Cerulean–expressing CT26HA tumors (blue) were implanted into the chambers, and animals were infused with GFP+ HA-Tregs (green). On day 7, mice were injected with tdTomato-expressing HA-CTLs (red); 2 days later, the behavior of both populations in tumor tissue was recorded by MP-IVM. (**A**) Overview highlighting position of T cells in both tumor stroma and parenchyma. (**B**) 3 sample time series of HA-Tregs that migrated in close vicinity of HA-CTLs without forming a stable interface suggestive of a direct interaction. Time shown in min:s. Scale bars: 100 μm (**A**); 10 μm (**B**).

also IL-2 produced by tumor-reactive Teffs. Tregs are more sensitive to IL-2 than the secreting Teffs due to their constitutively high expression of CD25, which allows them to respond faster to this limiting cytokine (50). In addition, indoleamine 2,3-dioxygenase is thought to contribute to Treg expansion in dLNs through an MHC-restricted mechanism in vitro (51).

In the current study, we used TCR transgenic Tregs recognizing a tumor cell–expressed model Ag as a surrogate for self-Ags expressed in tumor tissue in order to analyze the role of local Ag presentation to Tregs in controlling their activity. Our observation that sequentially transferred cohorts of Tregs each time first expanded in dLNs before infiltrating tumors supports the notion that Treg activation in LNs is needed for their deployment to effector sites. However, in addition to Ag-dependent activation of Tregs in dLNs, Ag presentation at the effector site was also necessary to sustain the local Treg response required to prevent CTL-mediated tumor rejection; such a requirement for ongoing Treg activation at effector sites may explain why tumor-infiltrating Tregs in cancer patients are more suppressive than their counterparts from the circulation, where they are not exposed to APCs (52). Interestingly, we found that Tregs expressed only low amounts of CD25 and failed to accumulate in tumors where they did not encounter their cognate Ag. This may reflect the cooperative control of CD25 expression by Foxp3 and the TCR-dependent transcription factor nuclear factor of activated T cells (NFAT) (35, 53). Without TCR stimulation and the resulting low expression of CD25, the high-affinity receptor for IL-2, Tregs may not only be compromised in their ability to utilize IL-2 produced by Teffs for their own survival and accumulation (32, 34), but also in their ability to control these cells by outcompeting them for available IL-2 (54).

It was unexpected that the clonal HA-Treg response in dLNs began to quickly decline about 1 week after tumor implantation. Interestingly, a paucity of Tregs in dLNs has also been observed in human ovarian cancer patients, especially at late tumor stages (7). However, polyclonal Tregs in dLNs of experimental mouse tumors tend to increase in number, at least over the first few weeks (48). We therefore hypothesize that our observation reflects the accelerated response of Tregs compared with Teffs (50), which results in faster egress and depletion from LNs in the absence of continuous recruitment of new HA-specific precursors.

Previous imaging studies on explanted tumor tissue and in vivo have shown that the interactions of CTLs with tumor cells and stromal APCs are heterogeneous with regard to their stability and duration (55–58). Here we compared the interactive behavior of Tregs and CTLs in both tumor parenchyma and stroma and found that Tregs migrated faster than CTLs in both environments and arrested significantly less frequently and for shorter periods of time than CTLs. In light of the generally low or absent expression of MHC II molecules by nonhematopoietic tumor cells, cognate Treg interactions in the epithelial tumor tissue studied here most likely occur with hematopoietic or other stromal APCs capable of taking up tumor cell–expressed Ags and presenting these via MHC II, rather than with the tumor cells themselves. Our visualization of Treg interactions with phagocytic cells and with CD11c+ DCs in both tumor parenchyma and stroma supports this notion.

How do Tregs cause CTL dysfunction? One possibility is that they inhibit tumor rejection through mechanisms unrelated to the expression of PD-1 and TIM-3 on CTLs, resulting in prolonged tumor Ag persistence, which in turn induces expression of these coinhibitory molecules on Teffs. However, in our experimental settings, CTLs also showed signs of dysfunction at time points when, even in the absence of Tregs, tumors are not yet undergoing rejection. Therefore, tumor load and thus Ag exposure were similar in these situations, which argues against this hypothesis.

Tregs have been proposed to operate both through core mechanisms of suppression, including IL-2 deprivation and CTLA-4–mediated downregulation of costimulatory molecules on APCs, and by diverse context-dependent mechanisms, including the secretion of cytokines, such as IL-10, IL-35, or TGF-β (59). Here we found that rapid downregulation of CD80 and CD86 on DCs (27, 28) occurred most effectively when Tregs encountered their cognate Ag on DCs in vitro. T cells are more migratory in vivo than in vitro, and Ag-dependent stabilization of Treg-DC contacts, as observed in our MP-IVM experiments, may therefore even be more important for promoting this mechanism of immunoregulation. The transient nature of their interactions with APCs may allow

motile Tregs to spread their regulatory activity more effectively in a larger volume of tumor tissue than if they formed more stable contacts. CTLs subsequently activated by such Treg-preconditioned DCs that had lost their costimulatory capacity showed enhanced coinduction of PD-1 and TIM-3, which may directly render them dysfunctional, or make them more susceptible to the induction of dysfunction through continued stimulation in a low CD80/86 context, where coinhibitory signals cannot be balanced by costimulatory signals (60). Interestingly, tumor-associated macrophages from human cancer patients also induce PD-1 and TIM-3 expression in autologous T cells (61), which suggests that this property is not limited to DCs.

A shared requirement for local Ag recognition by CTLs and Tregs in tumor tissue is in agreement with a scenario in which both cell types simultaneously or sequentially interact with the same APCs presenting their cognate Ags. These Ags may not need to be derived from the same cellular source, as in the present experimental system, but could for instance be tumor cell–expressed Ags in the case of CTLs, and self-Ags derived either from tumor cells or other sources in the case of Tregs. These Ags could still be presented jointly to both T cell types by the same APCs. A 3-cell model evoked by these considerations, in which an APC serves as a functional cellular bridge between Tregs and CTLs, is reminiscent of the interplay among Ag-presenting DCs, $CD4^+$ helper T cells, and $CD8^+$ cytotoxic T cells during the inductive phase of T cell responses (62). Given that several intravital microscopy studies, including the present one, have so far failed to generate evidence for direct, physical Treg interactions with Teffs during ongoing immune regulation in LNs (38, 63), such a 3-cell model has conceptual appeal, since it does not require direct Treg-CTL contact. This local functional interplay could also extend to $CD4^+$ Teffs, which are likely subjected to similar mechanisms of Treg-mediated control in the tumor environment (64, 65).

It will be interesting to investigate the role of $CD4^+$ Teffs in shaping CTL responses at effector sites. Apart from their CTL-independent effector functions, and in addition to facilitating CTL recruitment (1, 66), $CD4^+$ Teffs might also support CTL responses in direct antagonism to Tregs, by locally enhancing APC function (67). This implies that specialized APCs at effector sites may serve as local information hubs to integrate and relay immunostimulatory and immunoregulatory information among different classes of adaptive immune cells. Once identified, such effector site APCs may provide interesting targets for efforts to manipulate immune responses locally in a wide range of disease states where either improved or reduced immune effector function is desirable, with no or minimal systemic immune modulation. In the case of antitumor responses, this would require APCs with the ability to cross-present tumor Ags to CTLs, and our current efforts are aimed at further characterizing these APCs and their interactions with various T cell populations in tumor tissue.

Methods

Mice. CL4 mice express a transgenic TCR specific for H-$2K^d$/$HA_{515–523}$ (25). TCR-HA mice express a transgenic TCR specific for I-E^d/$HA_{107–119}$ (68). TCR-HA mice were crossed to pgk-HA transgenic mice, which express HA of influenza strain PR8 under the control of the phosphoglycerate kinase promotor (21). CL4 and TCR-HA×pgk-HA mice were crossed to either DPE-EGFP or T-Red transgenic mice expressing EGFP or DsRed2 in all T cells under control of a modified CD4 promoter (63). $Thy1.1^+$ BALB/c mice were originally obtained from P. Allen (Washington University, St. Louis, Missouri, USA). $Thy1.2^+$ BALB/c mice were from Jackson Laboratories. CD11c-mCherry transgenic mice on the B6 background (37) were bred to BALB/c animals, and F1 animals were used for experiments. All studies were performed on animals housed in specific pathogen–free conditions.

DNA constructs. PR8 HA was provided by R.J. Hogan (University of Georgia, Athens, Georgia, USA) as a pcDNA3.1 expression plasmid. Individual mutations (as described in the text and figure legends) were introduced by standard PCR site-directed mutagenesis. The open reading frames of WT and mutant HA were then cloned upstream of an IRES-$puromycin^R$ cassette into an HIV-1–based lentiviral vector originally developed in the Mulligan laboratory (69) to generate pHAGE-EF1α-HA (or mutant HA)-IRES-puro-W. A histone H2B-Cerulean fusion protein was provided by S. Megason (Harvard Medical School, Boston, Massachusetts, USA) as a pCS expression plasmid and cloned into the lentiviral vector to generate pHAGE-EF1α-H2B-Cerulean-W (without the IRES-$puromycin^R$ cassette). The open reading frames of H2B-mRFP1 and tdTomato were cloned into the retroviral vector pMSCVpuro (Clontech) to generate pMSCV-H2B-mRFP1 and pMSCV-tdTomato, respectively.

Tumor cell lines. The pHAGE-EF1α–based vectors described above were used to transduce the chemically induced carcinoma cell line CT26 (70) with HA (CT26HA) or various HA mutants, as well as with H2B-Cerulean (CT26, CT26HA, CT26HA F111D, CT26HA F111E, CT26HA Y516A, and CT26HA Y516D; all expressing H2B-Cerulean). H2B-Ceruelan expression allowed for the visualization of tumor cells by flow cytometry, histology, and MP-IVM (71). All CT26-derived lines were cultured in RPMI1640 supplemented with 10% FCS, glucose, penicillin, and streptomycin. Consistent expression of HA and HA mutants was ensured by regularly adding puromycin to the culture medium at 1 μg/ml.

Antibodies. The FITC- and allophycocyanin-tagged clonotypic 6.5 antibody, reactive with the TCR-HA receptor, was provided by H. von Boehmer (Harvard Medical School, Boston, Massachusetts, USA). The following commercial antibodies were used for immunophenotyping: anti-mouse CD4 (GK1.5), CD8α (53-6.7), CCR4 (2G12), CD11b (M1/70), CD11c (N418), CD25 (PC61), CD40 (3/23), CD44 (IM7), CD45 (30-F11), CD62L (MEL-14), CD69 (H1.2F3), CD80 (16-10A1), CD86 (PO3), CD103 (2E7), CD107a (1D4B), galectin-9 (RG9-35), Thy1.2 (30-H12), CD69 (H1.2.F3), TCR Vβ8.1/2 (MR5-2), IFN-γ (XMG1.2), Helios (22F6), I-A/I-E (M5/114.15.2), PD-1 (RMP1-30), PD-L1 (10F.9G2), PD-L2 (TY25), TIM-3 (B8.2C12), TNF (MP6-XT22) (all from Biolegend), TCR Vβ8.3 (1B3.3; BD Biosciences — Pharmingen), Foxp3 (FJK-16s; eBioscience), granzyme B (GB12; Caltag).

In vitro generation of HA-CTLs. Single-cell suspensions from spleens and LNs of CL4 mice were pulsed with 10 μM $HA_{515–523}$ peptide for 1 hour at 37°C, then cultured with 10 ng/ml murine rIL-12 for the first 2 days and 20 ng/ml murine rIL-2 (both cytokines from R&D Systems) for the following 5 days. For imaging experiments, HA-CTLs were transduced twice with either pMSCV-H2B-mRFP1 or pMSCV-tdTomato on days 1 and 2 after activation.

Enrichment of HA-Tregs. Single-cell suspensions from spleens and LNs of TCR-HA×pgk-HA mice were enriched for $CD4^+CD25^+$ T cells to >90% purity by negative immunomagnetic selection against CD8, B220, DX5, Ter119, and CD11b, followed by positive selection for CD25 expression ($CD4^+$ $CD25^+$ Regulatory T Cell Isolation Kit; Miltenyi Biotec). This population typically consists of 30%–40% of cells expressing CD25 and the HA-specific TCR TCR-HA, revealed by the clonotypic antibody 6.5. Alternatively, 99.8% pure HA-Treg populations were obtained by $CD4^+$ cell enrichment followed by fluorescence-activated cell sorting of $CD4^+CD25^+6.5^{hi}$ cells. Transfer of enriched and pure populations in numbers that contained comparable numbers of $CD4^+CD25^+6.5^{hi}$ cells (3×10^5 and 1×10^5, respectively) gave similar results in all aspects of the HA-Treg response investigated.

In vitro suppression assay. Enriched HA-Tregs and naive, CFSE-labeled (1 μM, 15 min) CL4 T cells were mixed at different ratios, and a constant

number of T cell–depleted BALB/c splenocytes was added as APCs. After addition of peptides $HA_{515–523}$ and $HA_{107–119}$ at 10 and 1 μM, respectively, cells were cultured for 3 days, with the addition of brefeldin A for the final 7 hours before flow cytometry analysis.

In vitro Treg conditioning of DCs. DCs were isolated from spleens by immunomagnetic selection using CD11c beads; activated in 10 ng/ml LPS; washed; cultured for 16 hours; pulsed with $HA_{107–119}$, $HA_{515–523}$, or both; and then cocultured at a 1:1 ratio with HA-Tregs. 3 hours later, HA-CTLs were added for a final DC/HA-Treg/HA-CTL ratio of 1:1:1 and cultured for an additional 12 hours before analysis.

In vitro reactivation of HA-CTLs with or without costimulation. HA-CTLs were cultured on different densities of plate-bound anti-CD3ε Abs (clone 145-2C11; Biolegend) for 12 hours with or without the activating anti-CD28 Ab (clone 37.51; Biolegend; plate-bound at 10 μg/ml).

Flank tumor implantation and growth measurements. Mice were inoculated s.c. in the right shaved flank or in both shaved flanks with 10^6 viable tumor cells suspended in 50 μl HBSS. Tumor size was determined by caliper measurements of tumor length and width, and tumor volume was calculated as $(l \times w^2)/2$.

FTY720 treatment. Several hours before adoptive transfer of HA-CTLs, recipient mice received i.p. injections of 1 mg/kg body weight FTY720 in sterile water or water alone. Injections were repeated every other day until the end of the experiment.

Tissue harvest for flow cytometric analyses. Tumor samples were trenched using razor blades and digested with 1.5 mg/ml collagenase D and 50 U/ml DNAse (both Roche) for 45 minutes at 37°C. Spleens and LNs were mechanically disintegrated. Splenocytes were also treated with ammonium chloride–based red cell lysis buffer. All tissue suspensions were passed through 40-μm filters before further treatment and again just before flow cytometric analysis.

Flow cytometry. Singe-cell suspensions were blocked with anti-CD16/32 Ab (clone 93; Biolegend) and incubated with fluorochrome-tagged antibodies for 30 minutes on ice. For detection of granzyme B, intracellular IFN-γ, and intracellular CD107a, cells were permeabilized and fixed using a commercial kit (Cytofix/Cytoperm; BD). For detection of Foxp3 and Helios, cells were permeabilized and fixed using a transcription factor staining buffer set (eBioscience). All flow cytometry analysis was performed on FACSCalibur, Accuri C6, or LSR II instruments (BD).

Tracking of transferred HA-Tregs and HA-CTLs in LNs and tumor tissue. In most cases, the CD4 Ag together with either the allelic marker Thy1.2 or EGFP expression were used to distinguish transferred HA-Tregs and HA-CTLs from endogenous T cells and from each other.

HA-Treg proliferation assay. Enriched HA-Tregs were incubated at 5×10^6 cells/ml with 5 μM CFDA, SE in PBS containing 0.1% FBS for 5 minutes at room temperature, washed first in PBS containing 20% FBS, counted, and resuspended in HBSS before injection into recipients.

Ex vivo CTL degranulation assay. To measure degranulation of HA-CTLs, enzymatically digested tumor single-cell suspensions were mixed on ice at 1:3 to 1:5 ratios with 10 μM $HA_{515–523}$ peptide–loaded splenocytes from healthy $Thy1.1^+$ BALB/c donors. Aliquots were pelleted in V-bottomed 96-well plates and resuspended in cold medium containing PE-labeled anti-CD107a antibody at 2 μg/ml. Degranulation of HA-CTLs was then triggered by rapidly warming the plates. Samples were removed, and the degranulation reaction was stopped by dilution in an excess of cold buffer at various time points for analysis by flow cytometry after additional surface staining for CD107a, Thy1.2, and CD4 on ice.

To measure degranulation of endogenous polyclonal CTLs, tumor single-cell suspensions were pelleted by centrifugation at 4°C onto the bottoms of 12-well plates coated with 10 μg/ml anti-CD3ε antibodies (clone 145-2C11; Biolegend). Degranulation was triggered by rapidly warming the plates. The reaction was stopped by dilution in an excess of cold buffer at 10 minutes for analysis by flow cytometry after additional surface staining for CD107a, Thy1, CD8, and CD4 on ice.

Ex vivo CTL cytokine production assay. Tumor single-cell suspensions were prepared as described above, and TNF and IFN-γ production was triggered for 4 hours by coculture with 1 μM $HA_{515–523}$ peptide–loaded BALB/c splenocytes, in the presence of brefeldin A during the last hour, followed by intracellular staining. Alternatively, for analyses of polyclonal CTLs, tumor single-cell suspensions were added for 4 hours to plates coated with anti-CD3ε antibodies, as described for the degranulation assay.

Histological analysis of T cell infiltration of tumors. Tumor samples were incubated in periodate-lysine-paraformaldehyde fixative overnight at 4°C, followed by successive dehydration in 10%, 20%, and 30% sucrose solution before freezing in OCT compound and preparation of 80-μm slices. Sections were directly analyzed without further staining. Signals detected in channel 1 (640–680 nm) were defined as autofluorescence and subtracted from other channels. From each tumor, multiple fields of view (614 × 614 μm) were randomly chosen at the stroma-parenchyma border zone, and 30- to 50-μm-thick volumes were recorded on a Prairie Technologies Ultima IV multiphoton microscope using an Olympus ×20/NA 0.95 water immersion objective lens.

MP-IVM. DSFCs were installed on mice as previously described (36, 72). 1–2 days later, mice were implanted with 2 aliquots of 10^6 H2B-Cerulean–expressing tumor cells each: one injected into the s.c. tissue exposed by the DSFC, the other s.c. into the scruff of the neck, in order to ensure continually robust lymphatic drainage of tumor tissue.

For visualization of HA-Tregs, mice were injected with $3–5 \times 10^5$ GFP^+ HA-Tregs on the same day of tumor implantation. To visualize HA-CTLs, 5×10^6 H2B-mRFP1– or tdTomato-expressing CTLs were injected into mice 7 days after tumor implantation. Tumor blood vessels were visualized by injection of 150 kDa TRITC-dextran or nonextravasating QDots655 (Molecular Probes). TRITC-dextran injection also led to labeling of phagocytic cells in tumor stroma and parenchyma.

Multiphoton excitation was obtained through DeepSee and MaiTai Ti:sapphire lasers (Newport/Spectra-Physics) tuned to 850 and 980 nm to excite all fluorescent probes used. Stacks of 11–12 square optical sections with 4- to 5-μm *z* spacing were acquired on an Ultima multiphoton microscope (Prairie Technologies) every 15–30 seconds to provide image volumes 40–55 μm in depth and 614 μm in width. Emitted fluorescence was detected through 460/50, 525/50, 595/50, and 660/40 band-pass filters and nondescanned detectors to generate 4-color images. Sequences of image stacks were transformed into volume-rendered time-lapse movies with Imaris software (Bitplane).

Cell motility analysis. Previously described parameters of cell motility (73) as well as the arrest coefficient (defined as the fraction of time an individual cell is immobilized; 4 μm/min threshold), were computed from Imaris-generated *xyzt* data using scripts written for MATLAB (Mathworks). To identify track segments characterized by low average speed (i.e., arrests), we computed the 3D instantaneous velocity moving average (7-point window) for all data points of individual cell tracks. An arrest was defined as a track segment characterized by averaged velocity below 4 μm/min for ≥2 minutes.

Statistics. Data were analyzed using Prism4 (GraphPad Software Inc.), and results were expressed as mean ± SEM for biological replicates and mean ± SD for technical replicates. 2-tailed Student's *t* test was used for comparisons of 2 groups, and ANOVA for comparison of 3 or more groups. A *P* value less than 0.05 was considered significant.

Study approval. All experiments described herein were approved by the IACUC of Massachusetts General Hospital.

Acknowledgments

We thank Ulrich von Andrian and James Moon for critical reading of the manuscript and helpful comments, and Sean Megason

and Jeff Hogan for the pCS-H2B-Cerulean and pcDNA3.1-HA constructs, respectively. T.R. Mempel was supported by NIH grants AI073457, CA150975, and CA179563 and by a grant by the Dana Foundation. C.A. Bauer was supported by a grant from the German Research Foundation (BA 3824/1-1). E.Y. Kim was supported by a Fellowship from the Terry Fox Foundation (Canadian Cancer Society Research Institute award no. 19726).

Received for publication February 17, 2014, and accepted in revised form March 20, 2014.

Address correspondence to: Thorsten R. Mempel, Massachusetts General Hospital – East, 149 Thirteenth Street, Room 8301, Boston, Massachusetts 02129, USA. Phone: 617.724.4596; Fax: 617.726.5156; E-mail: tmempel@mgh.harvard.edu.

1. Wong SB, Bos R, Sherman LA. Tumor-specific CD4+ T cells render the tumor environment permissive for infiltration by low-avidity CD8+ T cells. *J Immunol*. 2008;180(5):3122–3131.
2. Martin-Orozco N, et al. T helper 17 cells promote cytotoxic T cell activation in tumor immunity. *Immunity*. 2009;31(5):787–798.
3. Bos R, Sherman LA. CD4+ T-cell help in the tumor milieu is required for recruitment and cytolytic function of CD8+ T lymphocytes. *Cancer Res*. 2010; 70(21):8368–8377.
4. Corthay A, et al. Primary antitumor immune response mediated by CD4+ T cells. *Immunity*. 2005; 22(3):371–383.
5. Muranski P, et al. Tumor-specific Th17-polarized cells eradicate large established melanoma. *Blood*. 2008;112(2):362–373.
6. Boon T, Cerottini JC, Van den Eynde B, van der Bruggen P, Van Pel A. Tumor antigens recognized by T lymphocytes. *Annu Rev Immunol*. 1994;12:337–365.
7. Curiel TJ, et al. Specific recruitment of regulatory T cells in ovarian carcinoma fosters immune privilege and predicts reduced survival. *Nat Med*. 2004; 10(9):942–949.
8. Zippelius A, et al. Effector function of human tumor-specific CD8 T cells in melanoma lesions: a state of local functional tolerance. *Cancer Res*. 2004; 64(8):2865–2873.
9. Baitsch L, et al. Exhaustion of tumor-specific CD8(+) T cells in metastases from melanoma patients. *J Clin Invest*. 2011;121(6):2350–2360.
10. Sakuishi K, Apetoh L, Sullivan JM, Blazar BR, Kuchroo VK, Anderson AC. Targeting Tim-3 and PD-1 pathways to reverse T cell exhaustion and restore anti-tumor immunity. *J Exp Med*. 2010; 207(10):2187–2194.
11. Fourcade J, et al. Upregulation of Tim-3 and PD-1 expression is associated with tumor antigen-specific CD8+ T cell dysfunction in melanoma patients. *J Exp Med*. 2010;207(10):2175–2186.
12. Ahmadzadeh M, et al. Tumor antigen-specific CD8 T cells infiltrating the tumor express high levels of PD-1 and are functionally impaired. *Blood*. 2009; 114(8):1537–1544.
13. Brahmer JR, et al. Safety and activity of anti-PD-L1 antibody in patients with advanced cancer. *N Engl J Med*. 2012;366(26):2455–2465.
14. Topalian SL, et al. Safety, activity, and immune correlates of anti-PD-1 antibody in cancer. *N Engl J Med*. 2012;366(26):2443–2454.
15. Restifo NP, Dudley ME, Rosenberg SA. Adoptive immunotherapy for cancer: harnessing the T cell response. *Nat Rev Immunol*. 2012;12(4):269–281.
16. Josefowicz SZ, Lu LF, Rudensky AY. Regulatory T cells: mechanisms of differentiation and function. *Annu Rev Immunol*. 2012;30:531–564.
17. Weiss JM, et al. Neuropilin 1 is expressed on thymus-derived natural regulatory T cells, but not mucosa-generated induced Foxp3+ T reg cells. *J Exp Med*. 2012;209(10):1723–1742.
18. Malchow S, et al. Aire-dependent thymic development of tumor-associated regulatory T cells. *Science*. 2013;339(6124):1219–1224.
19. Vignali DA, Collison LW, Workman CJ. How regulatory T cells work. *Nat Rev Immunol*. 2008;8(7):523–532.
20. Wherry EJ. T cell exhaustion. *Nat Immunol*. 2011; 12(6):492–499.
21. Klein L, Khazaie K, von Boehmer H. In vivo dynamics of antigen-specific regulatory T cells not predicted from behavior in vitro. *Proc Natl Acad Sci U S A*. 2003;100(15):8886–8891.
22. Klein L, et al. Visualizing the course of antigen-specific CD8 and CD4 T cell responses to a growing tumor. *Eur J Immunol*. 2003;33(3):806–814.
23. Agata Y, et al. Expression of the PD-1 antigen on the surface of stimulated mouse T and B lymphocytes. *Int Immunol*. 1996;8(5):765–772.
24. Honda T, Egen JG, Lämmermann T, Kastenmüller W, Torabi-Parizi P, Germain RN. Tuning of antigen sensitivity by T cell receptor-dependent negative feedback controls T cell effector function in inflamed tissues. *Immunity*. 2014;40(2):235–247.
25. Morgan DJ, et al. CD8(+) T cell-mediated spontaneous diabetes in neonatal mice. *J Immunol*. 1996; 157(3):978–983.
26. Chen ML, et al. Regulatory T cells suppress tumor-specific CD8 T cell cytotoxicity through TGF-β signals in vivo. *Proc Natl Acad Sci U S A*. 2005; 102(2):419–424.
27. Wing K, et al. CTLA-4 control over Foxp3+ regulatory T cell function. *Science*. 2008;322(5899):271–275.
28. Qureshi OS, et al. Trans-endocytosis of CD80 and CD86: a molecular basis for the cell-extrinsic function of CTLA-4. *Science*. 2011;332(6029):600–603.
29. DiPaolo RJ, Brinster C, Davidson TS, Andersson J, Glass D, Shevach EM. Autoantigen-specific TGFbeta-induced Foxp3+ regulatory T cells prevent autoimmunity by inhibiting dendritic cells from activating autoreactive T cells. *J Immunol*. 2007;179(7):4685–4693.
30. Zhang N, et al. Regulatory T cells sequentially migrate from inflamed tissues to draining lymph nodes to suppress the alloimmune response. *Immunity*. 2009;30(3):458–469.
31. Smigiel KS, et al. CCR7 provides localized access to IL-2 and defines homeostatically distinct regulatory T cell subsets. *J Exp Med*. 2014;211(1):121–136.
32. Tang Q, et al. Central role of defective interleukin-2 production in the triggering of islet autoimmune destruction. *Immunity*. 2008;28(5):687–697.
33. Kim HP, Leonard WJ. The basis for TCR-mediated regulation of the IL-2 receptor α chain gene: role of widely separated regulatory elements. *EMBO J*. 2002;21(12):3051–3059.
34. Malek TR, Castro I. Interleukin-2 receptor signaling: at the interface between tolerance and immunity. *Immunity*. 2010;33(2):153–165.
35. Wu Y, et al. FOXP3 controls regulatory T cell function through cooperation with NFAT. *Cell*. 2006; 126(2):375–387.
36. Marangoni F, et al. The transcription factor NFAT exhibits signal memory during serial T cell interactions with antigen-presenting cells. *Immunity*. 2013;38(2):237–249.
37. Khanna KM, Blair DA, Vella AT, McSorley SJ, Datta SK, Lefrancois L. T cell and APC dynamics in situ control the outcome of vaccination. *J Immunol*. 2010; 185(1):239–252.
38. Tang Q, et al. Visualizing regulatory T cell control of autoimmune responses in nonobese diabetic mice. *Nat Immunol*. 2006;7(1):83–92.
39. Thornton AM, Shevach EM. Suppressor effector function of CD4+CD25+ immunoregulatory T cells is antigen nonspecific. *J Immunol*. 2000;164(1):183–190.
40. Romagnoli P, Hudrisier D, van Meerwijk JP. Preferential recognition of self antigens despite normal thymic deletion of CD4(+)CD25(+) regulatory T cells. *J Immunol*. 2002;168(4):1644–1648.
41. Hsieh CS, Liang Y, Tyznik AJ, Self SG, Liggitt D, Rudensky AY. Recognition of the peripheral self by naturally arising CD25+ CD4+ T cell receptors. *Immunity*. 2004;21(2):267–277.
42. Jordan MS, et al. Thymic selection of CD4+CD25+ regulatory T cells induced by an agonist self-peptide. *Nat Immunol*. 2001;2(4):301–306.
43. Apostolou I, Sarukhan A, Klein L, von Boehmer H. Origin of regulatory T cells with known specificity for antigen. *Nat Immunol*. 2002;3(8):756–763.
44. Wong J, Obst R, Correia-Neves M, Losyev G, Mathis D, Benoist C. Adaptation of TCR repertoires to self-peptides in regulatory and nonregulatory CD4+ T cells. *J Immunol*. 2007;178(11):7032–7041.
45. Kawahata K, et al. Generation of CD4(+)CD25(+) regulatory T cells from autoreactive T cells simultaneously with their negative selection in the thymus and from nonautoreactive T cells by endogenous TCR expression. *J Immunol*. 2002;168(9):4399–4405.
46. Nishikawa H, Sakaguchi S. Regulatory T cells in tumor immunity. *Int J Cancer*. 2010;127(4):759–767.
47. Fisson S, et al. Continuous activation of autoreactive CD4+ CD25+ regulatory T cells in the steady state. *J Exp Med*. 2003;198(5):737–746.
48. Darrasse-Jeze G, et al. Tumor emergence is sensed by self-specific CD44hi memory Tregs that create a dominant tolerogenic environment for tumors in mice. *J Clin Invest*. 2009;119(9):2648–2662.
49. Grinberg-Bleyer Y, et al. Pathogenic T cells have a paradoxical protective effect in murine autoimmune diabetes by boosting Tregs. *J Clin Invest*. 2010; 120(12):4558–4568.
50. O'Gorman WE, et al. The initial phase of an immune response functions to activate regulatory T cells. *J Immunol*. 2009;183(1):332–339.
51. Sharma MD, et al. Plasmacytoid dendritic cells from mouse tumor-draining lymph nodes directly activate mature Tregs via indoleamine 2,3-dioxygenase. *J Clin Invest*. 2007;117(9):2570–2582.
52. Strauss L, Bergmann C, Szczepanski M, Gooding W, Johnson JT, Whiteside TL. A unique subset of CD4+CD25^{high}Foxp3+ T cells secreting interleukin-10 and transforming growth factor-beta1 mediates suppression in the tumor microenvironment. *Clin Cancer Res*. 2007;13(15 pt 1):4345–4354.
53. Zheng Y, Josefowicz SZ, Kas A, Chu TT, Gavin MA, Rudensky AY. Genome-wide analysis of Foxp3 target genes in developing and mature regulatory T cells. *Nature*. 2007;445(7130):936–940.
54. Pandiyan P, Zheng L, Ishihara S, Reed J, Lenardo MJ. CD4+CD25+Foxp3+ regulatory T cells induce cytokine deprivation-mediated apoptosis of effector CD4+ T cells. *Nat Immunol*. 2007;8(12):1353–1362.
55. Mrass P, et al. Random migration precedes stable target cell interactions of tumor-infiltrating T cells. *J Exp Med*. 2006;203(12):2749–2761.
56. Breart B, Lemaitre F, Celli S, Bousso P. Two-photon imaging of intratumoral CD8 T cell cytotoxic activity during adoptive T cell therapy in mice. *J Clin Invest*. 2008;118(4):1390–1397.
57. Deguine J, Breart B, Lemaitre F, Di Santo JP, Bousso P. Intravital imaging reveals distinct dynamics for natural killer and CD8(+) T cells during tumor regression. *Immunity*. 2010;33(4):632–644.
58. Boissonnas A, Fetler L, Zeelenberg IS, Hugues S, Amigorena S. In vivo imaging of cytotoxic T cell

infiltration and elimination of a solid tumor. *J Exp Med*. 2007;204(2):345–356.
59. Wing JB, Sakaguchi S. Multiple treg suppressive modules and their adaptability. *Front Immunol*. 2012;3:178.
60. Chen L, Flies DB. Molecular mechanisms of T cell co-stimulation and co-inhibition. *Nat Rev Immunol*. 2013;13(4):227–242.
61. Dannenmann SR, et al. Tumor-associated macrophages subvert T-cell function and correlate with reduced survival in clear cell renal cell carcinoma. *Oncoimmunology*. 2013;2(3):e23562.
62. Castellino F, Germain RN. Cooperation between $CD4^+$ and $CD8^+$ T cells: when, where, and how. *Annu Rev Immunol*. 2006;24:519–540.
63. Mempel TR, et al. Regulatory T cells reversibly suppress cytotoxic T cell function independent of effector differentiation. *Immunity*. 2006;25(1):129–141.
64. Kryczek I, et al. Cutting edge: Th17 and regulatory T cell dynamics and the regulation by IL-2 in the tumor microenvironment. *J Immunol*. 2007; 178(11):6730–6733.
65. Li H, et al. Tim-3/galectin-9 signaling pathway mediates T-cell dysfunction and predicts poor prognosis in patients with hepatitis B virus-associated hepatocellular carcinoma. *Hepatology*. 2012; 56(4):1342–1351.
66. Nakanishi Y, Lu B, Gerard C, Iwasaki A. CD8(+) T lymphocyte mobilization to virus-infected tissue requires CD4(+) T-cell help. *Nature*. 2009; 462(7272):510–513.
67. Onishi Y, Fehervari Z, Yamaguchi T, Sakaguchi S. $Foxp3^+$ natural regulatory T cells preferentially form aggregates on dendritic cells in vitro and actively inhibit their maturation. *Proc Natl Acad Sci U S A*. 2008;105(29):10113–10118.
68. Kirberg J, Baron A, Jakob S, Rolink A, Karjalainen K, von Boehmer H. Thymic selection of $CD8^+$ single positive cells with a class II major histocompatibility complex-restricted receptor. *J Exp Med*. 1994;180(1):25–34.
69. Mostoslavsky G, Fabian AJ, Rooney S, Alt FW, Mulligan RC. Complete correction of murine Artemis immunodeficiency by lentiviral vector-mediated gene transfer. *Proc Natl Acad Sci U S A*. 2006; 103(44):16406–16411.
70. Brattain MG, Strobel-Stevens J, Fine D, Webb M, Sarrif AM. Establishment of mouse colonic carcinoma cell lines with different metastatic properties. *Cancer Res*. 1980;40(7):2142–2146.
71. Alexander S, Koehl GE, Hirschberg M, Geissler EK, Friedl P. Dynamic imaging of cancer growth and invasion: a modified skin-fold chamber model. *Histochem Cell Biol*. 2008;130(6):1147–1154.
72. Fukumura D, et al. Tumor induction of VEGF promoter activity in stromal cells. *Cell*. 1998; 94(6):715–725.
73. Sumen C, Mempel TR, Mazo IB, Von Andrian UH. Intravital microscopy; visualizing immunity in context. *Immunity*. 2004;21(3):315–329.